

Developing RAS-binding antibody-derived hit compounds

Shuyang Sun

MPhil thesis

Primary supervisor: Prof. Terry Rabbitts

Associate supervisor: Dr. John Caldwell

Word count: 10960

Abstract

The RAS family of proteins (comprising KRAS, NRAS and HRAS) are among the most often mutated proteins in human cancers, which are found in around 25% of all human tumours. It promotes the occurrence and maintenance of diseases through the interaction between RAS and effectors. Therefore, targeting RAS protein-protein interactions is expected to become an important therapeutic target. Earlier experiments obtained intracellular antibodies that blocked RAS protein-protein interaction, and screened a series of RAS-binding compounds overlapping the antibody-binding sites.

The aim of this project is the development of next generation of RAS-binding hits based on existing RAS-binding compounds to improve affinity and efficacy. In order to achieve this, RAS-binding compound Abd-7 was developed into Fluorescence Polarization (FP) probe by de novo synthesis of modified Abd-7 structure with benzylamine and addition of fluorophore sulfo-Cyanine5 (Cy5). Unfortunately, the modification of compounds had greatly changed the physical and biochemical properties of compounds and the fluorescence polarization biochemical assay could not be properly set up. This project attempts to validate whether FP probe-RAS interaction was impaired and to verify the possibility of streptavidin pull-down assay for drug discovery.

Abbreviations

Abd	Antibody-derived
Avi-Tag	A peptide allowing biotinylation by the enzyme BirA
Boc	<i>tert</i> -Butoxycarbonyl
BRET	Bioluminescence resonance energy transfer
CDR	Complementarity-determining region
CRAF	RAF proto-oncogene serine/threonine-protein kinase
cSPR	Competitive surface plasmon resonance
Cy5	Sulfo-Cyanine5
CYP	Cytochrome P450
DIPEA	N,N-Diisopropylethylamine
DLD-1	Human Dukes's type C colorectal adenocarcinoma cell line
DMF	Dimethylformamide
DMSO	Dimethylsulfoxide
EtOAc	Ethyl acetate
FP	Fluorescence polarization
FTase	Farnesyltransferase
GAP	GTPase activating protein
GDP	Guanosine diphosphate
GEF	Guanine nucleotide exchange factors
GGTase-I	Geranylgeranyltransferase-I
GppNHp	Non-hydrolyzable GTP analog
GTP	Guanosine triphosphate
HATU	(Dimethylamino)-N,N-dimethyl(3H-[1,2,3]triazolo[4,5-b]pyridin-3-ylloxy)methaniminium hexafluorophosphate
HEPES	4-(2-Hydroxyethyl)-1-piperazine ethanesulfonic acid
His-tag	Polyhistidine-tag
HPLC	High performance liquid chromatography
IC ₅₀	Half maximal inhibitory concentration
iDab	Intracellular single domain antibody
IgG	Immunoglobulin G
IPTG	Isopropyl 1-thio-beta-D-galactopyranoside

K _d	Equilibrium dissociation constant
LC-MS	Liquid chromatography-mass spectrometry
MAPK	Mitogen-activated protein kinase
MTT	3-(4,5-Dimethylthiazol-2-yl)-2,5-diphenyltetrazolium bromide
NF1	Neurofibroin
NF-κB	Nuclear factor kappa-light-chain-enhancer of activated B cells
NHS	<i>N</i> -Hydroxysuccinimide
NMR	Nuclear magnetic resonance
PI3K	Phosphoinositide 3-kinase
PVDF	Polyvinylidene fluoride
RaIGDS	Ral Guanine Nucleotide Dissociation Stimulator
SAR	Structure-activity relationship
SCX	Strong cation exchange
SDS-PAGE	Sodium dodecyl sulfate-polyacrylamide-based discontinuous gel
SOS	Son of Sevenless
STD	Saturation transfer difference
TCEP	Tris(2-carboxyethyl)phosphine hydrochloride
TEV	Tobacco etch virus
THF	Tetrahydrofuran
UV	Ultraviolet
VH	Heavy chain variable domain

Introduction

RAS biology

RAS, as a member of small G-proteins, is a family of related low-molecular-weight guanosine triphosphate (GTP)-binding proteins expressed in all animal cell lines, which can be divided into several families by evolutionarily conserved sequence. Although a superfamily of more than 170 RAS-related proteins has been identified¹, KRAS, NRAS and HRAS are among the most often mutated in human cancers, which are found in more than 30% of all human tumour cases^{2, 3}. HRAS and KRAS were first identified from transforming retroviruses (Harvey sarcoma virus and Kirsten sarcoma virus) in the 1960s^{4, 5}, while NRAS was discovered in human neuroblastoma cells by Robin Weiss's group at the Institute of Cancer Research⁶. These three members have 85% amino acid sequence identity and are all widely expressed, but subtle differences were still found. Many studies have proved that RAS isoforms cannot always replace each other. All three isoforms are widely expressed, but KRAS is expressed in almost all cell types and is imperative for mice growth⁷.

RAS proteins are guanine nucleotide binding molecules that work as binary molecular switch in signal transduction by guanosine triphosphate (GTP) binding and hydrolysis (figure 1). RAS is normally activated by growth factor receptors, including members of the epidermal growth factor receptor (EGFR) family and other extracellular stimuli. RAS protein activity in normal

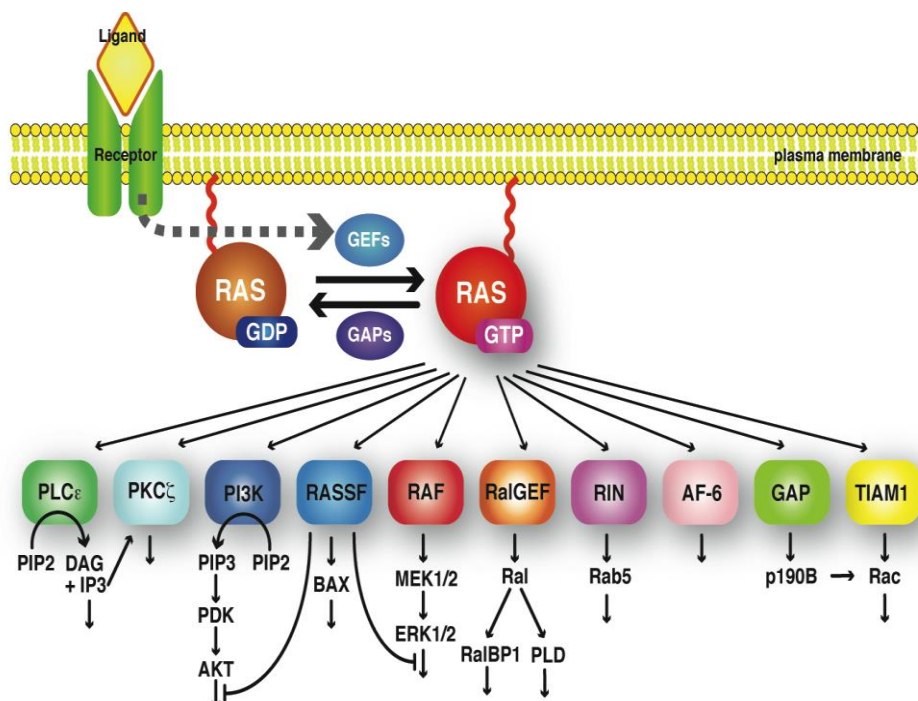


Figure 1. RAS cycle mechanism and pathway. Mutations of RAS can lead to the production of permanent activated RAS, which is GTP-bound. It can activate several downstream oncogenic signaling pathways such as PI3K and MAPK pathways and result in tumour cell growth (figure adapted from reference⁷⁶).

cells is controlled by the ratio of GTP to guanosine diphosphate (GDP)⁸. Although RAS has a low level of intrinsic GTPase activity and nucleotide exchange⁹, guanine nucleotide exchange factors (GEFs) (e.g., SOS1-2, RASGRF1-2, RASGRP1-4) and GTPase activating proteins (GAPs) (e.g., RASA1, RASA3-4, NF1, SYNGAP1) generally regulate the cycling between active and inactive states¹⁰⁻¹². GAPs accelerate GTP hydrolysis and RAS inactivation by activating GTPase activity of RAS protein. GEFs catalyse the release of GDP from RAS by breaking the interaction between P-loop and GDP. RAS binds to GDP in the inactivated state, while in the active state, RAS binds to GTP. Compared with GDP, GTP has an additional phosphate group, which induces conformational changes of two switch regions of RAS, known as switch I and switch II regions (figure 2) and activates the protein¹³. The balance between GEF and GAP activities determines the guanine nucleotide status of RAS and plays a decisive role in regulating normal RAS activity.

Interestingly, the RAS protein needs post-translational modification to locate on the correct subcellular compartment in order to play its biological activity, which usually results from lipid modifications to bind to the inner surface of the plasma membrane. Most RAS proteins

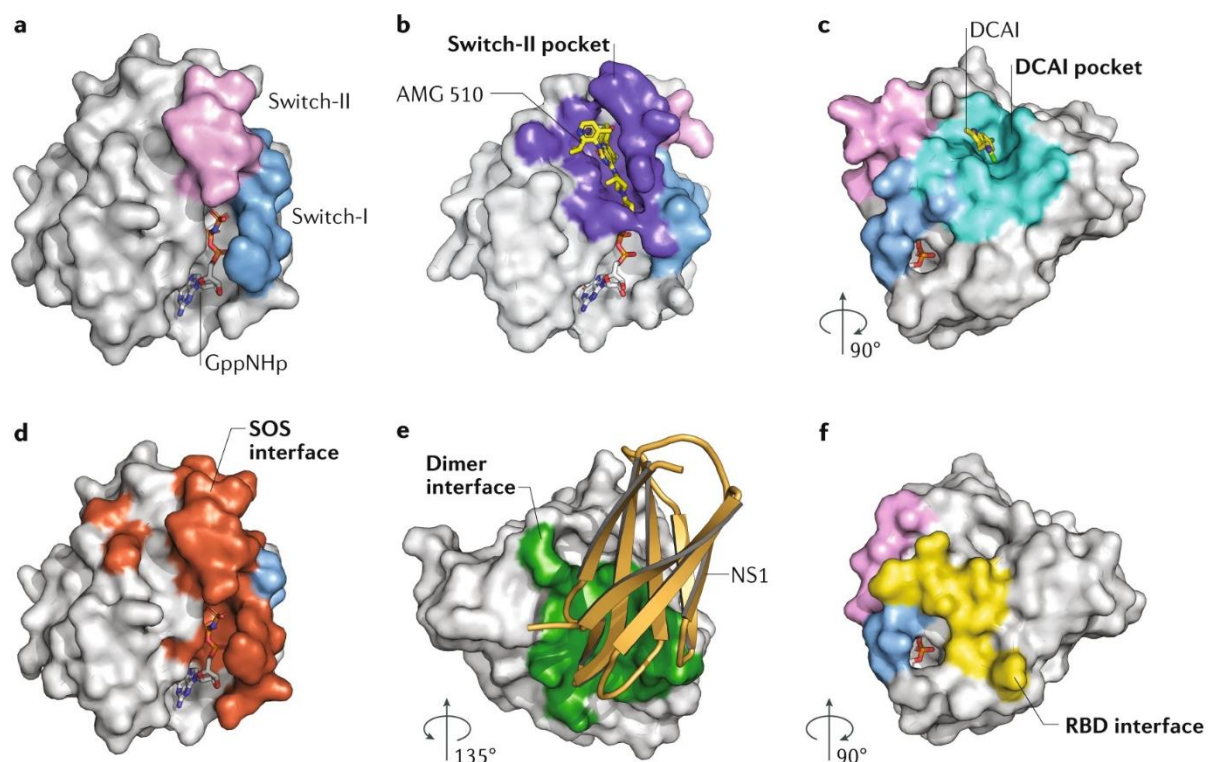


Figure 2. Surface representation of RAS structure a | HRAS bound to non-hydrolyzable GTP analog GppNHp (PDB: 5P21) b | KRAS-G12C bound to AMG 510 (PDB: 6OIM) c | KRAS-G12D bound to DCAI d | SOS binding interface of HRAS (PDB: 1BKD) e | Proposed HRAS dimerization interface bound by NS1 monobody (PDB: 5E95) f | RAS-RAF binding domain of HRAS (PDB: 4G0N) (figure adapted from reference⁴⁹)

covalently modify the C-terminal cysteine residues by geranylgeranylation or farnesylation¹⁴⁻¹⁶.

GTP-bound RAS with high affinity for RAS-effectors is involved in intracellular signal transduction by inducing downstream signal cascades such as RAF proto-oncogene serine/threonine-protein kinase (ARAF, BRAF, and CRAF) pathway^{17, 18}, phosphoinositide 3-kinase (PI3K) pathway¹⁹ and RAS-like guanosine diphosphate dissociation stimulator (RALGDS) pathway^{20, 21}, which are key signalling pathways for regulation of a variety of cell behaviors such as cell proliferation, differentiation, apoptosis, adhesion, migration and actin cytoskeleton integrity by different combinations of protein–protein interactions. RAS-RAS dimer formed by GTP-bound KRAS4B protein has been found to promote the dimerization and activation of RAF kinase and block interactions from other effectors²².

Activated RAS leads to the activation of the PI3Ks, which phosphorylates phosphatidylinositol 4,5-diphosphate (PtdIns(4,5)P₂) and converts to phosphatidylinositol 3,4,5-triphosphate (PtdIns(3,4,5)P₃) as the second messenger²³⁻²⁵. Third phosphate group of PIP₃ simultaneously recruits kinase PDK1 (adenosine 3-phosphate dependent protein kinase-1) and AKT (protein kinase B (PKB)) to the plasma membrane, leading to activation of AKT. AKT promotes cell survival and resists apoptosis by phosphorylating various targets of downstream regulatory pathway²⁶. PI3K can activate Rac (a subfamily of the Rho family of GTPases) as well, which is also important in RAS induced transformation and promotes activation of nuclear factor kappa-light-chain-enhancer of activated B cells (NF- κ B) (a transcription factor that controls cell proliferation and cell survival)²⁷⁻²⁹.

The human RALGEF family consists of four different proteins: RALGDS, RALGDS like protein 1 (RGL1), RGL2/RLF and RGL3. All members of the RALGDS family are effectors of RAS because they are all involved downstream of RAS signalling such as in RAS-dependent cell-cycle adjustment, cell apoptosis, cell transformation and cytoskeletal organization^{19-21, 30}.

RAS isoforms

There are three RAS genes (HRAS, NRAS and KRAS) in the human genome, encoding four RAS proteins with 188 to 189 amino acids (HRAS, NRAS, KRAS4A and KRAS4B)¹. Due to the alternative fourth exon utilization, KRAS encodes two splice variants KRAS4A and KRAS4B proteins due to alternative splicing of distinct 4th exons^{31, 32}. RAS protein has been found to have 82 to 90% of the total amino acid sequence identity and 93 to 99% of the sequence identity in the conserved N-terminal G domain (residues 1 to 164)^{33, 34}, which

consists switch I, switch II, and a P loop. Different isoforms show a high degree of identity in the relevant sequences that interact with the GDP-GTP cycle and activate downstream effectors, while only 8% of the sequence identity (residues 165 to 184/185) is shown in the C-terminal hypervariable region (HVR) and the four last amino acids CAAX motif. Difference in C-terminals leads to different posttranslational lipid modifications, resulting in unique membrane binding (including the CAAX introduced farnesylation, the lysine-rich sequence of KRAS and the palmitoylation of cysteine residues of the CAAX sequence of HRAS and NRAS) and transport dynamics of each isoform³⁵⁻³⁷. Other characteristics may be due to differences of isoforms in gene expression or distinct non-overlapping lipid microenvironments on the cytoplasmic face³⁸. Therefore, although the structure and biochemistry of the four RAS protein subtypes are almost the same, each RAS subtype has overlapping but different localization on the plasma membrane and inner membrane, participates in different activator and effectors, and plays different biological functions and cancer driving roles^{33, 39-42}.

HRAS, KRAS and NRAS proteins are widely expressed, but KRAS is expressed in almost all cell types. Gene knockout studies in mice show that KRAS is the most important RAS isoform for normal development and KRAS ablation mice die during embryogenesis^{7, 43}. The HRAS (-/-)/NRAS (-/-) double-knockout mice show normal growth, fertility and neuronal development⁴³. HRAS replacement of KRAS results in normal embryonic development despite cardiovascular pathology in adult mice⁴⁴. In contrast, NRAS is involved in the antiviral immune response and T cell function of mice and not important for the development, growth and reproduction⁴⁵. These studies show that different RAS subtypes play a unique role by participating in different signal transduction pathways.

RAS mutations

RAS gene is the most common mutation oncogene family in human cancer, which occurs in more than 30% of all human cancer cases, with 98% of the mutations from three mutational codon sites: G12, G13 and Q61^{2, 3, 33, 46}. Codons 12 and 13 are located in one of the four key sequence regions for GTP-binding, while Codon 61 is located in sequence regions for GTP-binding and GEF-binding (switch II)⁴⁷. Mutations of RAS in codon 12 block the GTPase activity of RAS and decrease the rate of GTP hydrolysis, while mutations in codon 61 accelerate the rate of GDP-GTP exchange. These mutations prevent GTP hydrolysis and lead to the production and accumulation of permanently activated GTP-bound RAS, which activates downstream oncogenic signaling pathways (e.g. MAPK and PI3K pathways), promotes pro-survival and pro-proliferative signaling and results in tumour cell growth.

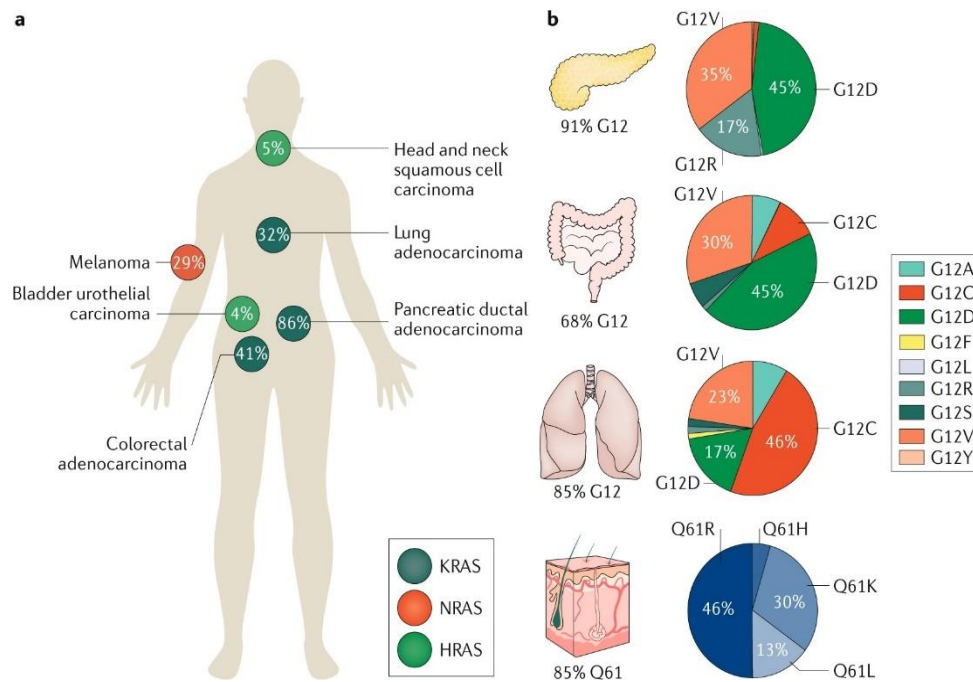


Figure 3. a| Frequency and distribution of RAS mutations by isoform in human cancers b| Distribution of RAS mutations with different mutated codons and their amino acid substitutions (figure adapted from reference⁴⁹)

Despite the high similarity among the three isoforms, each mutation of particular isoforms and residues shows preferential pairing with a specific cancer type⁴⁸. KRAS is the main mutation of RAS isoforms in human RAS cancer (85%), followed by NRAS (11%), and HRAS is the least (4%). KRAS mutations occurs frequently in 32% of lung adenocarcinoma, 86% of pancreatic ductal adenocarcinoma and 41% of colorectal adenocarcinoma⁴⁹ (figure 3). Within all KRAS mutant tumours, 80% of carcinogenic mutations originate from codon 12, among which mutation G12D is the most important variant (35%), followed by G12V (29%), G12C (21%)⁵⁰⁻⁵². Unlike KRAS, mutations in codon 61 of NRAS mutation happens in 29% of melanoma cases. HRAS mutations are relatively rare, and they mainly occur in bladder and head and neck squamous cell carcinoma⁴⁹. In multiple myeloma, RAS mutations are found in about 40% of cases, of which just over half are KRAS mutations³³.

The mutation frequency of each residue and isoform varies according to different cancer types and substitution of different amino acids may have different oncogenic abilities and biological functions. For example, Ink4a-deficient mice with NRASQ61R but not NRASG12D shows melanoma development⁵³. Therefore, many RAS-induced cancers originate from different RAS mutations, and a universal anti-RAS cancer treatment cannot be applied to all RAS mutation cancers⁵⁴. Instead, the selective treatment method must be tailored according to specific isoforms and mutations. The effects of RAS mutations of different carcinogens on cancer patients still need further study.

In the absence of mutant RAS, amplification or overexpression of wild-type RAS genes may promote tumours by the absence of negative regulatory factors or the upregulation of positive regulatory factors^{19, 55, 56}. The loss of negative regulatory factors such as GAPs is important for cancer activated by wild-type RAS. For example, the deletion of neurofibroin (NF1), one of the important GAPs, leads to excessive activation of RAS in tumour cells and triggers type I neurofibrotosis⁵⁷. RAS signaling pathway can be also activated by upregulation of positive regulatory factors such as EGFR and ERBB2, including breast cancer, ovarian cancer, gastric cancer and lung cancer^{58, 59}. Wild-type RAS protein is sometimes found to promote tumour when mutant RAS has different isoforms. For example, it shows that rhabdomyosarcoma with NRAS mutation may need wild-type KRAS or HRAS to activate and maintain⁶⁰. Unexpectedly, wild-type RAS proteins sometimes play an important role of tumour promotion or tumour inhibition in tumourigenesis, tumour maintenance and metastasis^{33, 56}. Although in a few cases, the wild-type RAS has a tumour promoting effect in the context of the homologous mutation RAS⁶¹, most studies have shown that the wild-type RAS is more likely to show a tumour suppressive effect in tumours driven by homologous mutation RAS isoforms.

Development of RAS inhibitors

For many years, RAS was considered as "undruggable" and there have been many problems in the development of effective therapies to inhibit RAS-effector interaction. Firstly, the traditional view is that RAS lacks a deep pocket outside the nucleotide binding pocket, while hydrophobic shallow pockets are more difficult to bind tightly with small molecules^{62, 63}. Second, RAS has picomolar affinity for guanine nucleotide, which is not conducive to the competitive binding of nucleotide analogues⁶⁴. Therefore, many of the RAS inhibitor studies are looking for alternative approaches.

Although KRAS is essential for the development of mice, studies have found that when KRAS is replaced by HRAS, mice can survive, which reduces the consideration of the toxicity of targeted KRAS drug⁴⁴. KRASG12C mutation is a mutational hotspot in KRAS and makes up about 13% of non-small cell lung cancer, 3-5% of colorectal cancer, and 1-2% of many other solid tumours⁶⁵. A library of 480 tethering compounds was screened based on disulfide bond fragments to determine their covalent binding to KRASG12C⁶⁶. Crystallographic research has discovered a new pocket underneath the switch II that bound to the effector, and the KRASG12C inhibitor developed based on this switch II pocket. In 2019, one covalent KRASG12C inhibitor named AMG 510 was approved by FDA (figure 4a)⁶⁷. Unlike other codon mutations, KRASG12C showed intrinsic GTPase activity close to the wild type, which gave

some compounds the opportunity to covalently bind GDP-bound KRASG12C^{68, 69}. The covalent inhibitor was designed to target the cysteine-12 of GDP-bound KRASG12C with the quinazoline core occupying the switch II pocket and blocking SOS-catalysed nucleotide exchange⁶⁶. Cellular potency of the initial hit was then improved by introducing different phenyl/pyridine substituents to occupy the adjacent H95/Y96/Q99 pocket (figure 4b). AMG 510 was finally determined by testing cellular potency, permeability, solubility and oral bioavailability of different structures. AMG510 has good tolerance, excellent pharmacological properties and significant tumour inhibition ability of KRASG12C in vivo, which endows it with great value for further clinical research⁷⁰. The good anti-tumour efficiency of AMG510 promotes its combined use with other targeted or cytotoxic drugs to improve the efficiency in vitro and in vivo⁷¹. Despite this promising discovery, for KRAS mutants other than G12C, this method may still have relevance for targeting on cysteine-185⁷² and histidine-95 in KRAS, but it is not universal. The discovery of previously unknown binding pockets and the development of the first switch II pocket inhibitor covalently bound to RAS mutants represent an important step in targeting RAS.

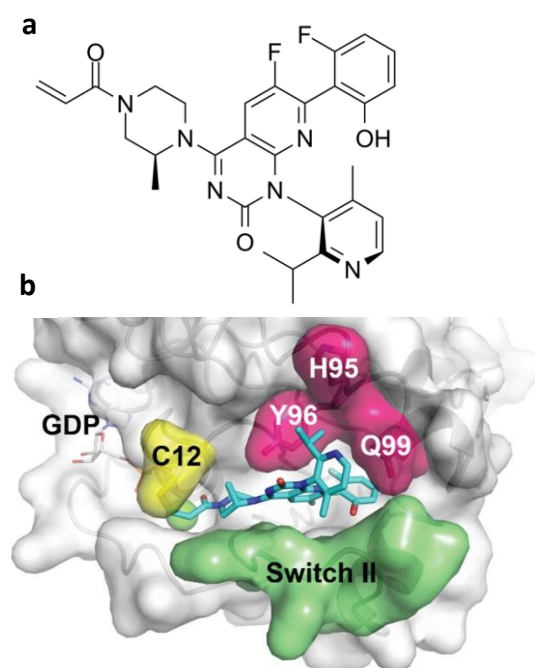


Figure 4. a | Structure of AMG 510 b | X-ray crystal structure of compound AMG 510 bound to GDP-KRASG12C (PDB: 6OIM)

Table 1. List of inhibitors targeting mutant RAS

Inhibitor	Designed target	Clinical trial identifier	Stage	Discovered year
AMG510	KRASG12C	NCT03600883	FDA approval	2018
MRTX849	KRASG12C	NCT03785249	FDA approval	2019
JNJ-74699157	KRASG12C	NCT04006301	Phase I	2019
D-1553	KRASG12C	NCT04585035	Phase I/II	2020
GDC-6036	KRASG12C	NCT04449874	Phase I	2020
LY3537982	KRASG12C	NCT04956640	Phase I	2021
JDQ443	KRASG12C	NCT04699188	Phase I/II	2021
BI 1823911	KRASG12C	NCT04973163	Phase I	2021
JAB-21822	KRASG12C	NCT05002270	Phase I/II	2021
MK-1084	KRASG12C	NCT05067283	Phase I	2021
RMC-6291	KRASG12C	NCT05462717	Phase I	2022
RMC-6236	Multi-RAS	NCT05379985	Phase I	2022
MRTX1133	KRASG12D	NCT05737706	Phase I/II	2023

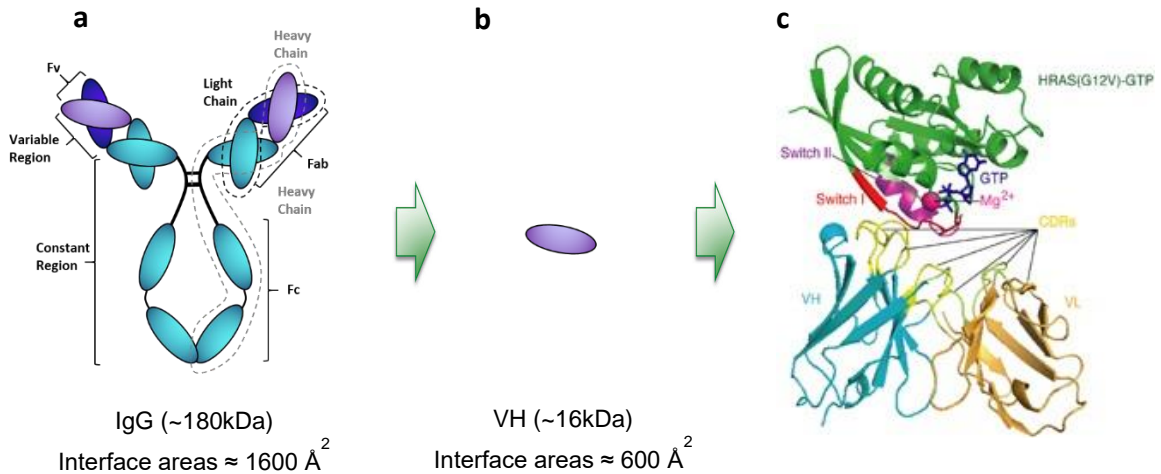


Figure 5. Antibody fragment that binds to activated RAS isoforms. Compared with traditional IgG (a), it was found that the variable domain VH (b) still showed a good binding affinity but better intracellular stability and penetration ability. Crystal structure of HRASG12V protein complexed with the scFv format of iDab#6 is shown in ribbon form (c). HRASG12V is shown in green and the RAS switch I & II regions are in red and purple respectively. The Fv proteins VH and VL are shown in cyan and orange respectively with their CDRs shown in yellow and lemon separately (figure adapted from reference⁷⁵).

Blocking RAS-effector (e.g. CRAF, RalGDS and PI3K) interaction to disrupt downstream signal transduction provides a direct and single idea for the treatment of mutant RAS cancers. Small molecule drugs can easily penetrate cells, but their ability to interfere with PPI is always questioned due to low affinity and smaller surface area for interactions. Macrodrugs were then introduced as an alternative to small molecules. This work started with implementation of intracellular antibody technologies^{73, 74}. Compared with traditional IgG, it was found that the variable domain VH still showed a good binding affinity but better intracellular stability. Some intracellular antibody fragments with higher affinity than endogenous effectors have been developed to successfully block RAS-GTP effect interaction sites, demonstrating the effectiveness of RAS-effector PPI inhibition^{75, 76}. Rabbits team obtained a novel single domain VH iDab#6 that specifically bound to the switch region of GTP-bound RAS with high affinity⁷⁷ and inhibited tumourigenesis and metastasis in a RAS mutated mouse model by blocking the RAS-effector interaction surface, which was shown in crystallography^{75, 78}. The interaction between iDab#6 and mutant HRAS proteins was at least 10 times higher than with wild-type HRAS. However, the study of drug delivery related to the internalization of macromolecular drugs into cells has always been a challenge. Macromolecule drugs largely suffer from poor metabolic stability and low bioavailability, which may hinder their clinical therapeutic application⁷⁹. Using target validated macromolecules to screen small compounds that bind to the target at the same location can greatly reduce target areas of the protein in competitive screening and increase the likelihood of identifying potential candidates. The binding site of a VH comprises around 600 Å² on average while the value of IgG is around 1600 Å², which is

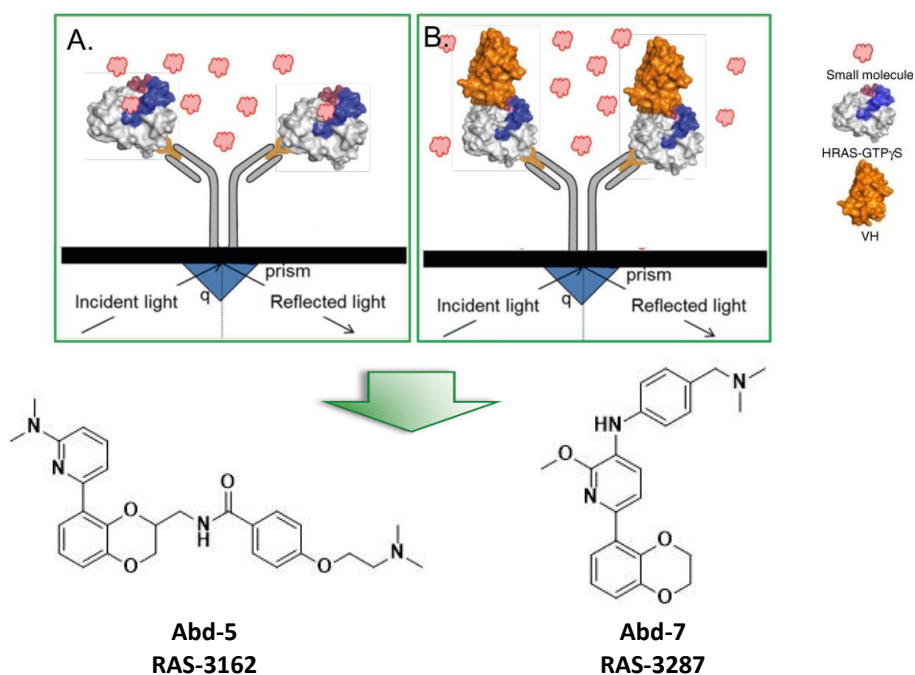


Figure 6. Competition SPR identifies RAS-binding compounds. SPR can specifically identify compounds bound to GTP-HRASG12V mutant through differential binding by detecting changes in reflected light angle. RAS-binding compound 3162 and 3287 are the two representative compounds of a series of RAS-binding chemical fragments (figure adapted from reference⁸³).

suitable for competitive screening of small molecule libraries (figure 5)⁸⁰⁻⁸². iDab#6 was applied as a competitor in a screen of a chemical fragment library to select compounds binding to RAS at the cognate site by competitive surface plasmon resonance (cSPR)⁸³. The initial hit was optimised to obtain antibody-derived small molecules (Abd-) series with improved biophysical properties and better K_d in 2018. High-resolution crystal structures show the binding of a chemical series of compounds to mutant RAS in the same hydrophobic pocket close to the switch regions I and II. Among the series, Abd-7 showed an improved *in vitro* KRAS affinity ($K_d = 51$ nm) and the phosphorylation of ERK and AKT of KRAS downstream was inhibited in cell assay (figure 6). Similar results were observed in RAS inhibitor series Ch- developed by Rabbits team, which bound to a pocket where compound Abd-7 was developed and showed a very similar binding mode to Abd-7⁸⁴ (figure 7).

BI-2852, published in 2019, also bound in a shallow pocket between the switch I and II regions with a GTP-KRASG12D affinity K_d 740 nm (figure 7). It was found that BI-2852 leads to inhibition of downstream signal

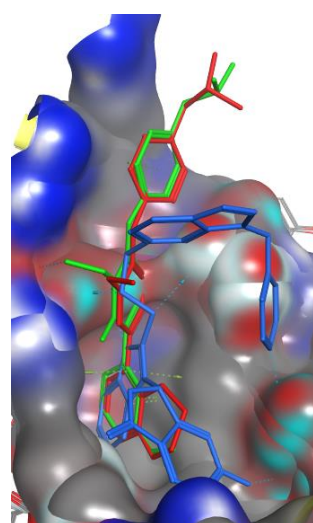


Figure 7. Alignment of RAS-3287 (red) (PDB: 6FA4), Ch-3 (PDB: 6GQY) and BI-2852 (PDB: 6GJ7) in KRASG12D pocket

transduction and antiproliferation in KRAS mutant cells in the low micromolar range by inhibiting both SOS1-catalysed and GAP-catalysed GTP-GDP exchange in KRAS as well as RAS effectors CRAF and PI3K α ⁸⁵.

Inhibiting RAS-GEF interaction to reduce the formation of GTP-RAS is another research hotspot, mainly referring to inhibiting the exchange function of Son of Sevenless (SOS, an important GEF) or its scaffold protein SHP2⁴⁹ (figure 2d). Small molecules that bind to KRAS between Switch I and Switch II and inhibit SOS binding and SOS mediated nucleotide exchange have been researched. A small ligand named DCAI was discovered by fragment screen to bind to a hydrophobic RAS pocket ($K_d = 1.1 \pm 0.5$ mM) (figure 2c) and weakly inhibit RAS-SOS1 interaction⁸⁶. Another early RAS-SOS inhibitor BAY-293 selectively inhibits the KRAS–SOS1 interaction with an IC₅₀ of 21 nM, but preferred to inhibit wild-type KRAS rather than mutant KRAS⁸⁷. It was reported that SOS1-KRAS inhibitor BI-3406 effectively reduced the formation of GTP-RAS and the proliferation of many KRAS driven cancer cells *in vitro* and *in vivo*^{88, 89}. SHP2, as a scaffold protein that binds GRB2 and SOS1, is involved in facilitating RAS nucleotide exchange and is necessary to activate the MAPK pathway^{90, 91}. An SHP2 inhibitor SHP099 stabilises SHP2 in an auto-inhibited conformation and is observed to improve KRAS mutant tumours *in vivo*^{92, 93}. The modified SHP2 inhibitor RMC-4630 exhibits a 67% disease control rate in patients with advanced NSCLC with KRAS mutations, and is currently undergoing a phase I single drug clinical trial⁹⁴. SHP2 allosteric inhibitors such as JAB-3068 are also undergoing phase I/II clinical trials to analyse the safety and antitumour activity of KRAS mutant solid tumours.

The biological effect of RAS relies on its membrane localisation. The covalent connection of the farnesyl isoprene group to the carboxyl terminal CAAX motif of RAS protein is crucial for the localization of RAS onto the plasma membrane. An indirect inhibition by targeting farnesyltransferase (FTase) was tried in the 1990s⁹⁵⁻⁹⁸. However, research showed that FTase inhibitors (FTI) only had a good inhibitory effect on HRAS⁹⁹ while the clinical performance of FTI in KRAS mutant cancers was disappointing. KRAS and NRAS can be partially modified to keep their membrane association by substitution of geranyl geranyl transferase (GGTase) that KRAS does not possess⁹⁹. Also, the simultaneous inhibition of FTase and GGTase-I was fatal to mice^{96, 100}. These two enzymes act on many different substrates, while inhibition can lead to toxicity to normal tissues⁹⁵. Other post-translational modifications of inhibitors are mainly directed towards RAS converting enzymes (RCE1) that target the cleavage terminal AAX residue downstream of the isopentenylated RAS protein and isoprenoylcysteine carboxymethyltransferase (ICMT) that methylates the cysteine residue of the CAAX box.

Targeting downstream RAS effectors is an alternative approach for RAS inhibition. RAF kinases (ARAF, BRAF, and CRAF) are involved in RAS-RAF-MEK-ERK signaling. Clinically approved BRAF-V600 inhibitors such as vemurafenib and dabrafenib have instead been shown to drive the dimerization of BRAF and CRAF to paradoxically activate the MAPK pathway in RAS mutant tumours¹⁰¹. Some pan-RAF inhibitors such as lifirafenib and Belvarafenib are observed to have therapeutic potential for RAS mutations^{102, 103}. MEK inhibitors do not show the same paradoxical pathway activation as RAF and have shown activity in patients with NRAS mutant melanoma¹⁰⁴, but there is no significance in MEK inhibition of KRAS mutant tumours¹⁰⁵. Due to the insufficient efficacy of MEK monotherapy, the possibility of combined treatment with upstream and downstream related inhibitors is being explored in clinical practice¹⁰⁶. The development of ERK inhibitors is relatively late but may have some potential¹⁰⁷. The preclinical ERK inhibitor SCH-772984 reduced phosphorylated ERK levels and cell proliferation in RAS mutant cancer cell lines and induced tumour regression in mouse models with KRAS or NRAS mutations^{107, 108}. However, the clinical compound MK-8353 based on SCH-772984 has not found tumour improvement in patients with KRAS or NRAS mutations in the phase I single drug treatment clinical trial of MK-8353¹⁰⁹. In a phase I clinical trial, BVD-523 (ulixertinib) showed therapeutic efficacy for NRAS mutant melanoma¹¹⁰.

The PI3K-AKT-mTOR pathway is another RAS related signal pathway. RAS activates the PI3K and MAPK pathways, and there is a complex feedback mechanism. Inhibition of one pathway can lead to compensatory activation of the other. Therefore, inhibiting MAPK and PI3K is a feasible strategy, which was proved by preclinical experiments^{111, 112}. However, in clinical trials, the combination of PI3K and MEK inhibitors has poor tolerance and efficacy¹¹³, and further research is needed on the dosage regimen or inhibitors.

Aims of the project

Although initial antibody-derived RAS-binding compounds were successfully achieved with promising affinity *in vitro*, the previous study observed discrepancy between affinity (*in vitro* K_d) and efficacy (IC_{50} in cells). Within Abd- series, Abd-5 (*in vitro* $K_d = 220$ nM) had an effect on the viability of DLD-1 KRAS-G13D cell line ($IC_{50} = 20$ μ M at 72 h), while the most potent compound is Abd-7 (*in vitro* K_d is 51 nM) with an IC_{50} of 8 μ M in DLD-1 at 72 h, still showing a >100-fold drop off in potency between *in vitro* and cell-based study⁸³. There are several possible explanations such as non-specific binding in the cell, compound stability and high conformational variability of RAS^{114, 115}. Biophysical K_d measured by cSPR may not be

representative of the binding affinity in the cellular environment and the affinity and efficacy of RAS-binding compounds may require further improvement.

The aim of this project is the development of next generation of RAS-binding hits based on existing RAS-binding compounds to improve affinity and efficacy for pre-clinical assay. The *in vitro* nanomolar binding affinity of Abd-7 to RAS makes it an attractive starting point for the development of RAS inhibitors. In order to achieve this, RAS-binding compound Abd-7 was designed and developed into Fluorescence Polarization (FP) probe by de novo synthesis of modified Abd-7 structure and crosslinking of fluorophore sulfo-Cyanine5 (Cy5). It is expected to establish a FP assay to identify available RAS compounds with the same binding site but improved efficacy and develop a SAR understanding based on biochemical activity perspective. Unfortunately, the fluorescence polarization biochemical assay could not be properly set up because the fluorophore modification of compounds had greatly changed the physical and biochemical properties of compounds, resulting in a significant decrease in compound affinity. This project attempts to validate whether FP probe-RAS interaction was impaired and to verify the possibility of competitive streptavidin bead pull-down strategy to detect binding compounds to the binding site for drug discovery.

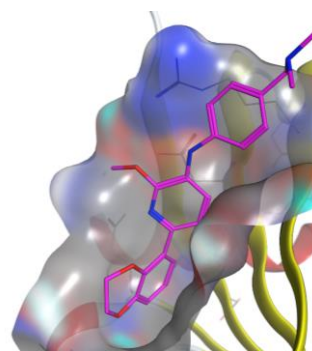


Figure 8. High resolution crystal structure of RAS-binding compound 3287 binding to KRAS (PDB: 6FA4)

Results and discussion

Choice of fluorochrome

The selection of fluorescent dyes is crucial in FP determination. Previous studies have shown that different fluorescent groups have a significant impact on the affinity of small molecule drugs and even antibodies to their receptors^{116, 117, 118}. Taking adenosine A1 receptor ligands as an example, previous studies synthesized different fluorescent derivatives of the archetypal Adenosine A1 receptor antigen found that the difference in potency between different modifications could reach up to 10 times, Modifications of antagonist XAC with BODIPY-FL did not even show specific binding at high concentrations¹¹⁷.

There are many options for FP fluorochrome, such as green-emission fluorophores (ATTO 488, Alexa 488, fluorescein), yellow-emission fluorophores (TAMRA, Cy3B), red-emission fluorophores (Alexa 647, Cy5)¹¹⁹. Their excitation and emission spectra must be different from the wavelengths of other molecules present in the solution to reduce the impact of

spontaneous fluorescence of compounds on experimental results¹²⁰. Related studies identified a large number of small molecules with fluorescence characteristics in the spectrum, and found that the blue shift wavelength is the severely affected area where the fluorescence characteristics of most small molecules overlap with commonly used fluorescent groups while the overlap is significantly reduced in the dark shift region exceeding 550 nm^{121 122}. Fluorescence intensity (RFU) of red-emission Cyanine5 is independent of the pH condition. We also expect the sulfonated analogue of cyanine5 can improve the inherent poor hydrophilicity of cyanine. Therefore, a red fluorophore sulfo-Cyanine5 was selected as the first choice to reduce false negatives derived from spontaneous fluorescence emitted in the green and blue ranges, as well as false positives caused by light scattering events. Green-emission fluorophore ATTO 488 was also introduced in this project as a comparison and alternative solution. ATTO 488 is a hydrophilic fluorescent label with good water solubility. The dye exhibits strong absorption, high fluorescence quantum yield and better thermal and photostability. The reaction with ATTO 488 does not change the reactants and the reaction conditions are similar to those for Cy5.

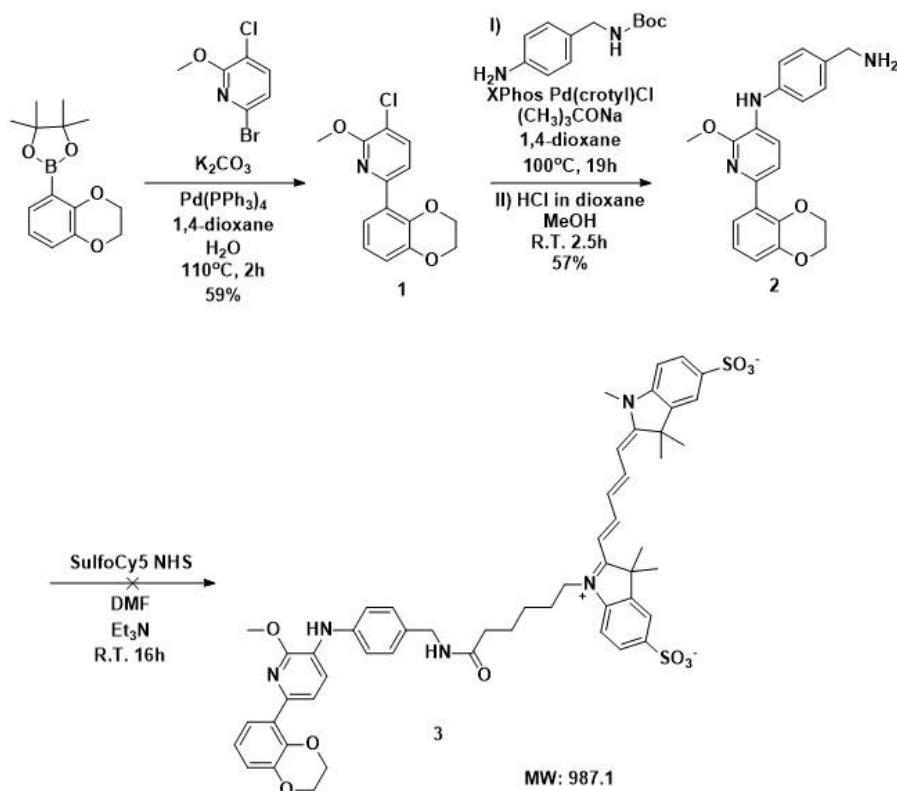
Probe Design

The ideal fluorescent probe design for inhibitors should retain the high affinity and selectivity of the parent ligand. High resolution crystal structure shown of compound RAS-3287 combined with KRAS guides the design of FP probe.

Although the structure-activity relationship shows that although the terminal tertiary amine of RAS-3287 and the adjacent phenyl ring have a better competitive effect on the RAS effectors due to the steric hindrance, high resolution crystal structure indicates that the modification of the terminal amine may not have a significant impact on key binding site (a pocket adjacent to the RAS switch regions I and II). Therefore, compound RAS-3287 substituted by terminal primary amine would be synthesized and react with NHS ester-activated crosslinkers of the fluorophores to obtain objective probes.

Synthesis of FP probe

Synthesis of FP-RAS-3287



Scheme 1. Synthesis of FP-RAS-3287

The first aim of this project is the development of antibody-derived small molecules into FP probes. As is shown in scheme 1, the synthesis of FP-RAS-3287 began from Suzuki coupling¹²³ of boronic ester to obtain 3-chloropyridine **1**, followed by Buchwald coupling¹²⁴ to obtain Boc intermediate. Then the Boc group was removed to obtain benzylamine **2**, and the NHS-ester of the fluorescent dye reacted with primary amine to give the amide formation **3**.

It was shown on figure 9 that a strong UV peak with mass ion 988 (M + H) and 1010 (M + Na) can be observed at 1.45 min in reaction mixture after 17 h. HPLC analytical separation was then carried out on a Phenomenex Kinetex C18 column. The mobile phase was a mixture of methanol and water both, containing formic acid at 0.1%. Due to high dilution after purification, only weak signal was detected on UV/MS of HPLC of the collected fractions. Based on characteristic of blue visualization of the Cy5 probe, all the fractions with blue colour were

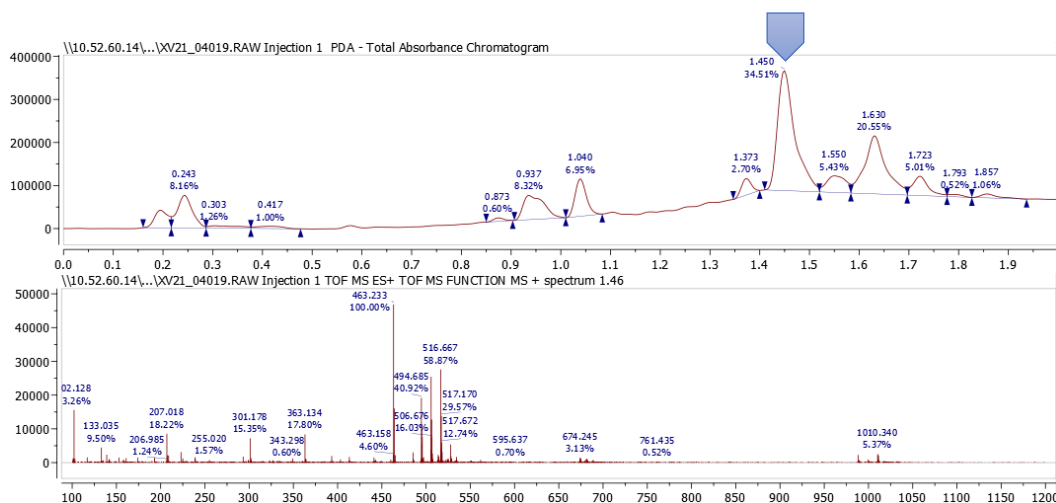
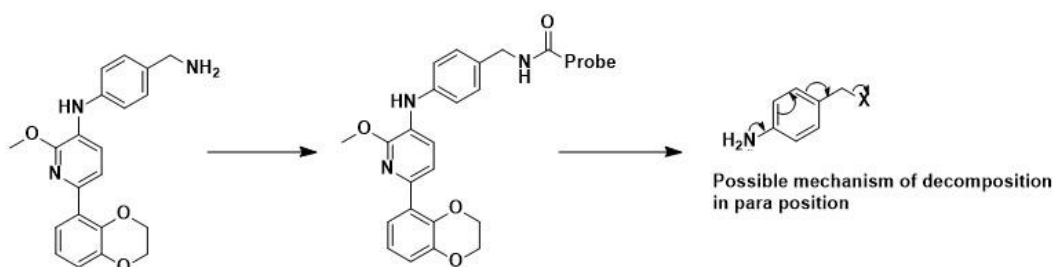


Figure 9. LC-MS of FP-RAS-3287 amide formation reaction mixture



Scheme 2. Speculation of instability of FP-RAS-3287. Electron transfer of the para position might involve in decomposition.

collected and tested by LC-MS. However, no peak with relevant mass ion was observed due to particularly high dilution after purification. Higher concentration was then achieved by combination of adjacent fractions with blue colour and evaporation by rotary evaporator with 40 mbar for 2 h. The concentrated fraction was then sent for LC-MS analysis but no peak with relevant mass ion was observed either. The stability of the compound was considered as a potential risk. One possible speculation was that the electron transfer from the para position lone pair of electrons was involved in decomposition (scheme 2).

The stability trial was carried out by incubating the crude reaction mixture in acidic condition (10% formic acid in MeOH) and neutral condition (MeOH only) separately (figure 10). It was observed that the intensity of the UV peak of the objective compound decreased over time, which implied that FP-RAS-3287 might not be stable and could decompose in both acidic condition and neutral condition spontaneously.

Two improved structures were proposed (scheme 3) and implemented to remove the interference of electron transfer caused by the para-aminomethylaniline structure.

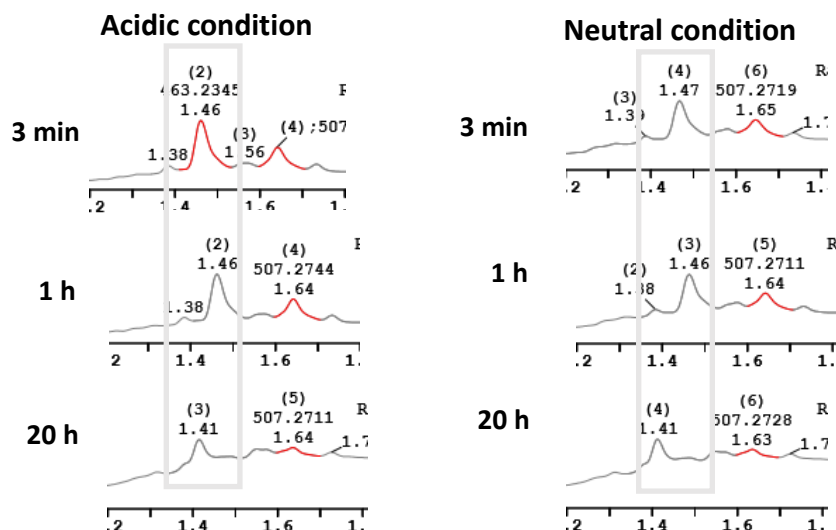
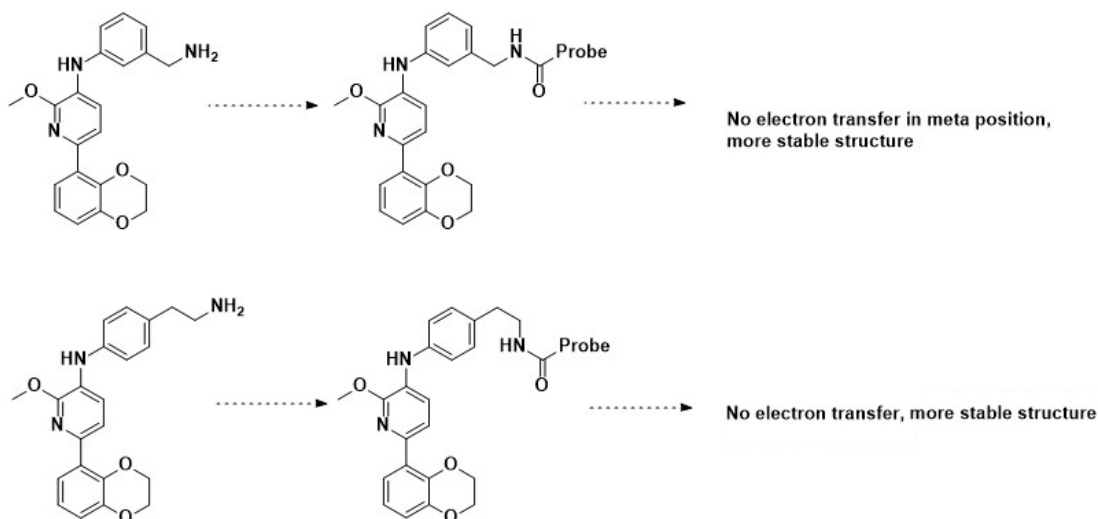


Figure 10. LC-MS of FP-RAS-3287 in acidic condition group (10% formic acid in MeOH) and neutral condition group (MeOH only) over time



Scheme 3. Two different structures with improved stability. The interference of electron transfer was removed.

Synthesis of FP-RAS-3287-2

The synthesis and purification of FP-RAS-3287-2 applied the same methodology as its para version. It was shown on figure 11 that a related and strong UV peak with mass ion 988 ($M + H$) can be observed at 1.4 min in reaction mixture after 20 h. However, the first purification was unsuccessful. No peak with relevant mass ion was observed in any of the fractions nor the concentrated combined fractions. Dr. John Caldwell repeated the final step of synthesis and improved the purification process. Unlike previous HPLC purification, this time the reaction mixture was loaded in DMSO and Biotage® Sfär C18 Reversed Phase

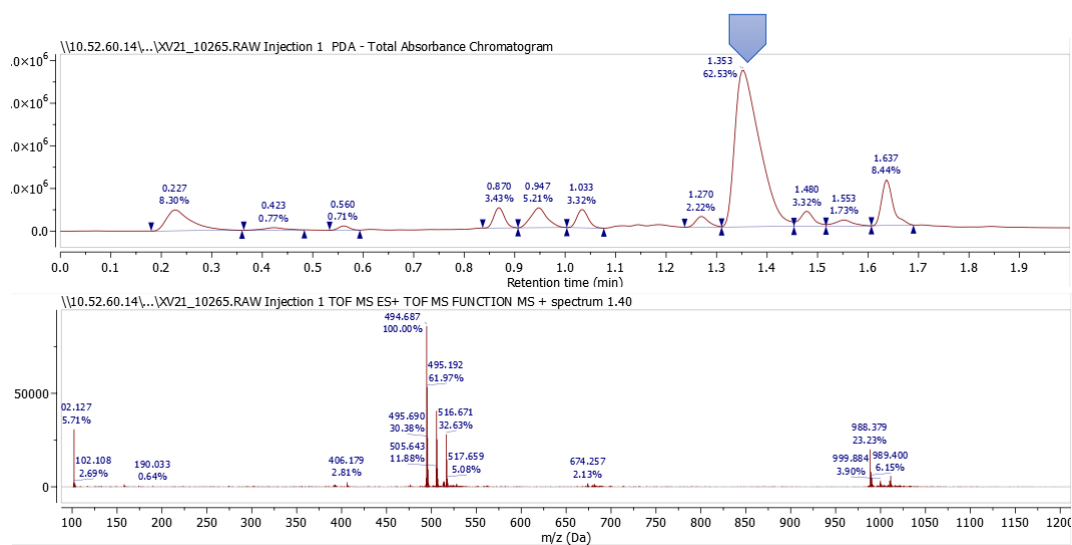
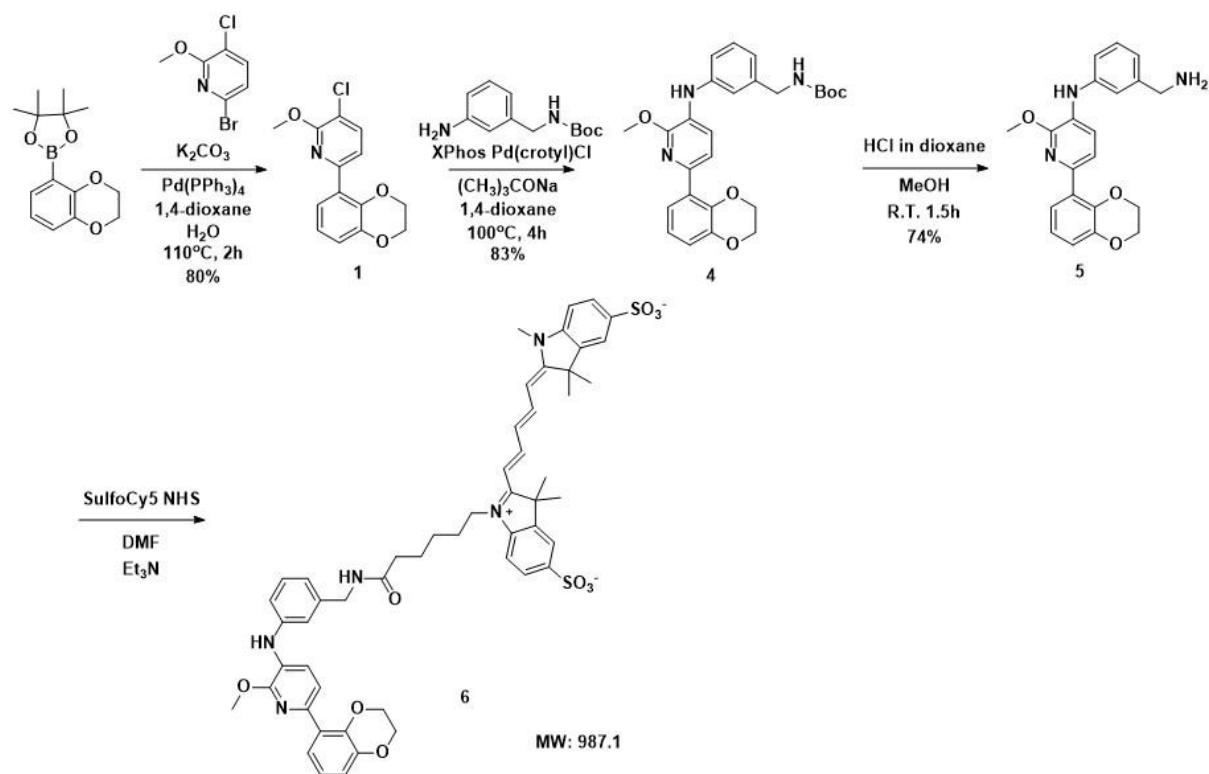
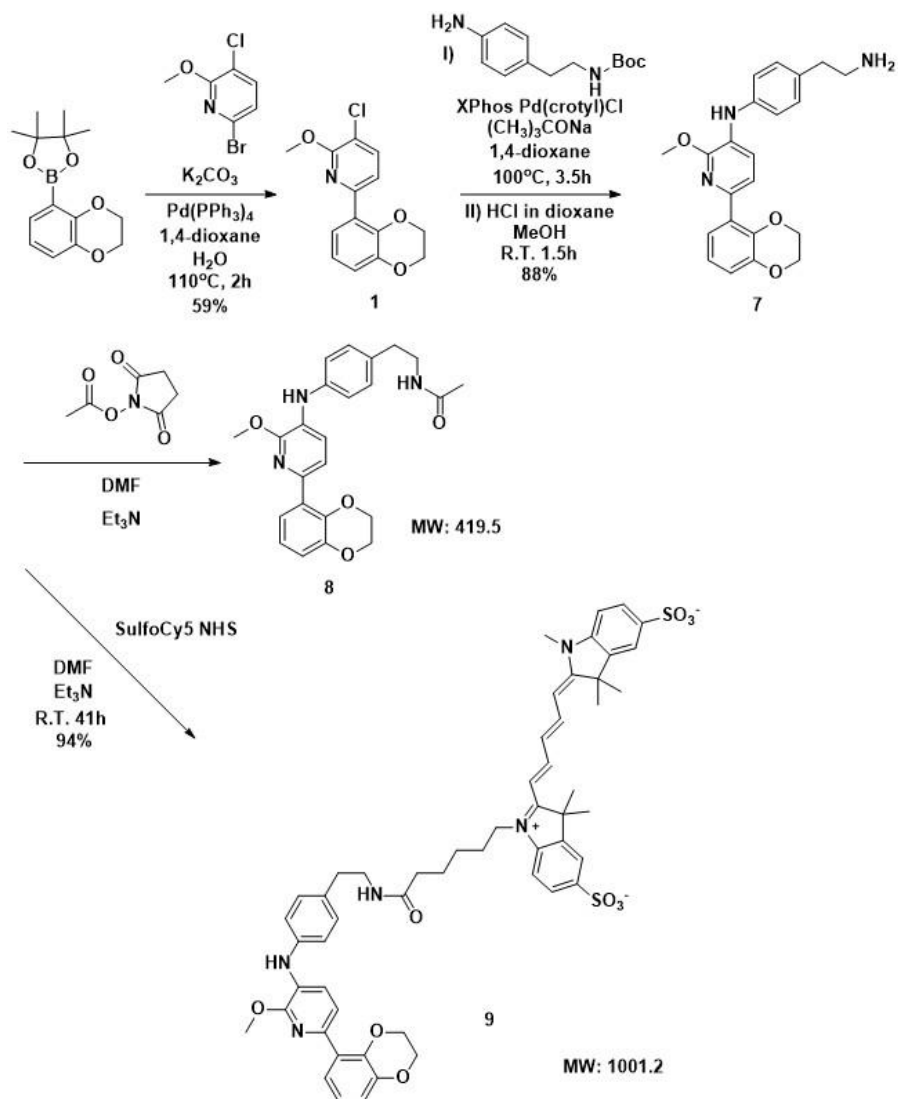


Figure 11. LC-MS of FP-RAS-3287-2 amide formation reaction mixture

chromatography was applied for better real-time control of the purification process and testing of the composition of each fraction, followed by SCX-2 purification. The collected $^1\text{H-NMR}$ data shows that the purification was successful. Although some DMSO was detected, it should not affect its use as a FP probe.

Synthesis of FP-RAS-3287-3

The synthesis and purification of FP-RAS-3287-3 followed the same methodology as other FP-RAS-3287 compounds. A simple compound 2,5-Dioxopyrrolidin-1-yl acetate was used to



Scheme 5. Synthesis of FP-RAS-3287-3

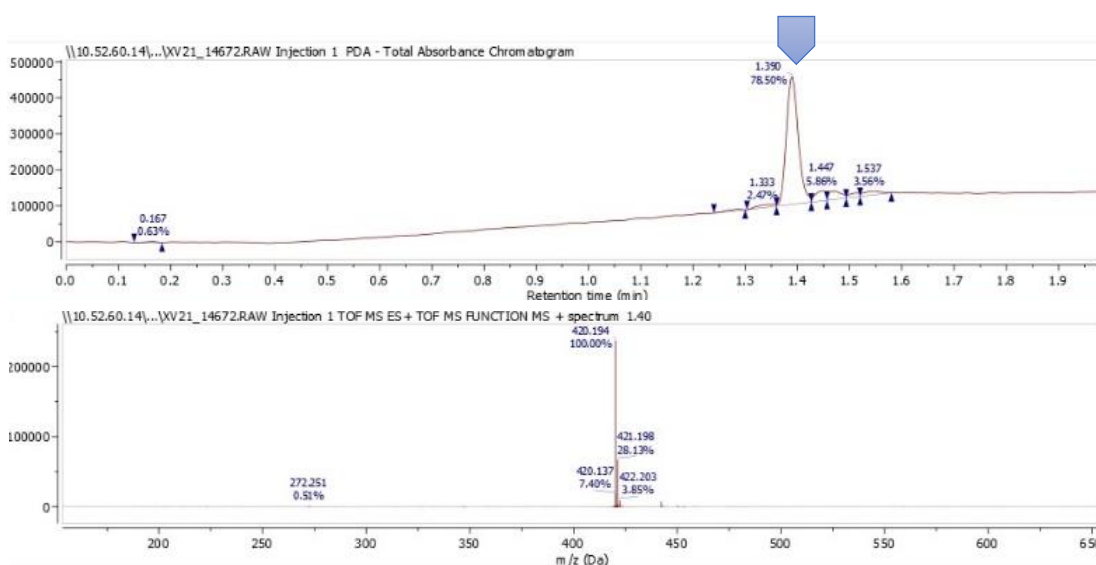


Figure 12. LC-MS of HPLC purified compound 8

simulate the amide formation process between NHS ester Cy5 and amine and verify the

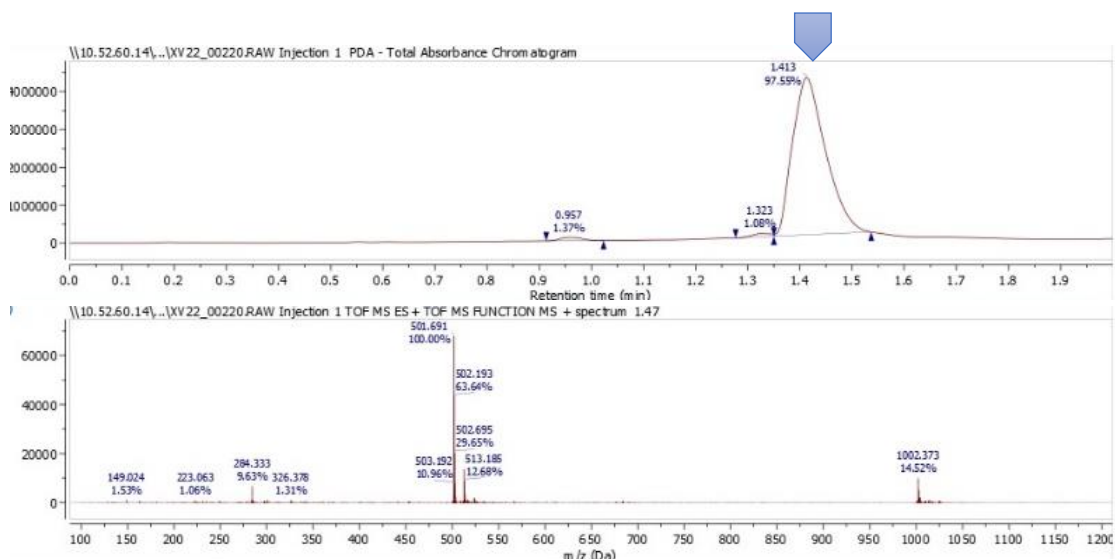


Figure 13. LC-MS of HPLC purified compound 9

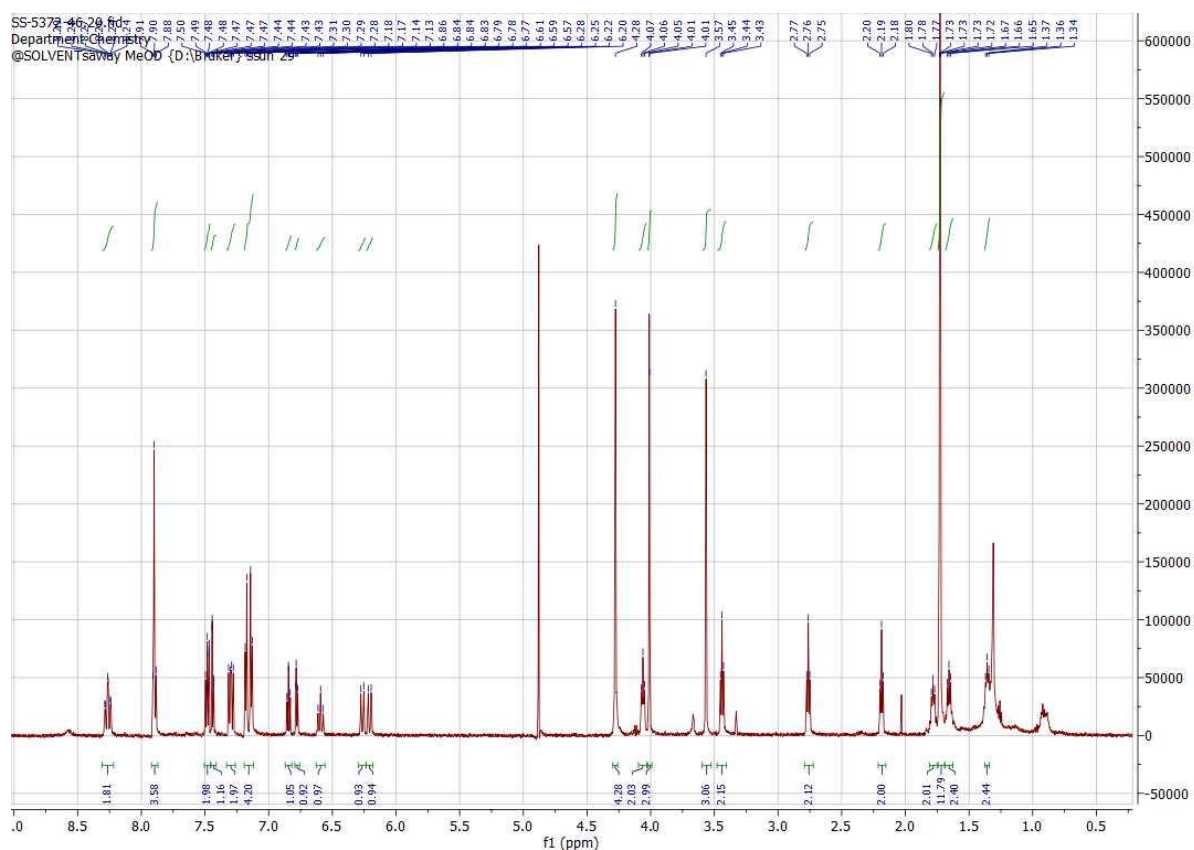


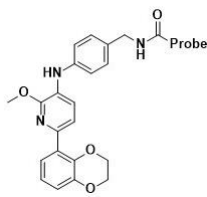
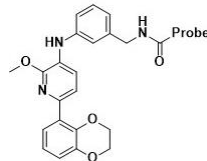
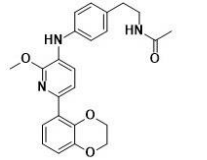
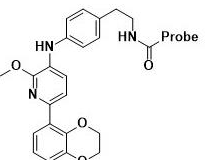
Figure 14. ^1H NMR (solvent away mode) of HPLC purified compound 9

stability of the hit part. Compound **8** was synthesised under the same reaction conditions as compound **9**, purified by HPLC purification with 1 x extended gradient elution (40% to 100% MeOH) and verified by LC-MS (figure 12). Compound **9** was then synthesised and eluted in HPLC with 2 x extended gradient elution (40% to 100% MeOH) and 2 x washing (100% MeOH). The purified product was verified and characterised by LC-MS and NMR (figure 13&14). It was shown on figure 13 that a single UV peak with mass ion 1002 ($M + H$) can be observed at 1.47 min.

Summary of FP-RAS-3287 series

The first proposed FP-RAS-3287 was considered a potential unstable structure, possibly due to 1,4 electron transfer. However, the subsequent model FP-RAS-3287-2 improved the stability, but still failed to be isolated. The simplified model confirmed that the RAS-hit part of improved structure can be stable in water/MeOH solution and Cy5 was considered to be stable. Although possible instability was eliminated, in terms of purification condition needed to isolate FP-RAS-3287-3, it indicates that both lipid solubility and water solubility of FP-RAS-3287-3 were reduced after coupling with Cy5. By improving loading skill and the purification method, FP-RAS-3287-2 was also separated from the reaction mixture. The synthesis experience shows that our understanding of products is still insufficient. In addition to the optimization of purification conditions, it should be noted that the significant solubility issues of FP-RAS-3287 series observed in purification may have serious risk to negatively affect subsequent FP assay development.

Table 2. A summary of FP-RAS-3287 series

Name	Structure	Comments
FP-RAS-3287		1.Weak MS signal was detected in reaction mixture 2.Unable to purify by HPLC 3.Poor stability
FP-RAS-3287-2		1.Improved MS signal in reaction mixture 2.Purified by Biotage® Sfür C18 Reversed Phase + SCX-2 and verified by crude NMR and LC-MS
FP-RAS-3287-3-Simplified testing model		1.Improved MS signal in reaction mixture 2.Easy HPLC separation
FP-RAS-3287-3		1.Successfully synthesised, purified and verified by NMR and LC-MS 2.Poor solubility

Attempt to synthesize FP-RAS-3287 with ATTO fluorophore

The initial idea was to introduce ATTO probe as a comparison and alternative solution for Cy5 probes (figure 15), and to investigate the impact of different fluorescent groups on FP experiments. The experiment was conducted by Dr. John Caldwell, using compound **7** as the reactant and planning to quickly synthesize the target compound through a one-step reaction combined with the more efficient Biotage® Sfür C18 Reversed Phase chromatography and SCX-2 purification combination. Although product formation was observed by LC-MS, the exceptionally broad peak in LC-MS (figure 16) suggests it has very poor solubility. Due to the suspected poor solubility, attempts to purify the product further failed.

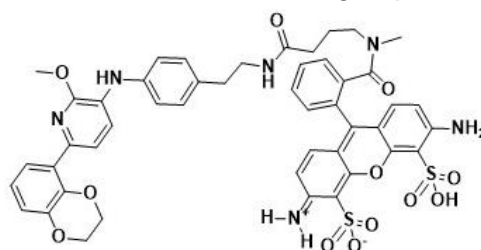


Figure 15. Proposed structure of FP-RAS-3287 with ATTO fluorophore

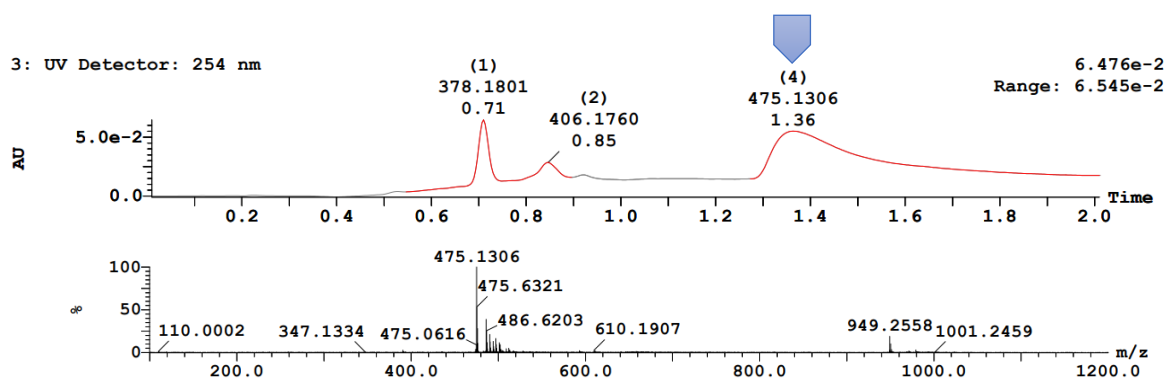


Figure 16. LC-MS of FP-RAS-3287 with ATTO fluorophore reaction mixture

Protein expression and purification

Recombinant RAS proteins were prepared for FP assay and crystallography analysis. His-tag, comprised of six histidine residues, is fused to the N terminus of RAS proteins and used for protein purification by forming coordination bonds with transition metal ions, which is too small and does not interfere with interactions between protein and protein/small molecules in most cases. TEV tag was designed for cleavage of His-tag after purification if necessary. Avi-tag was introduced for biotinylation and biotinylated RAS protein can be bound to streptavidin chips for SPR screening¹²⁵.

The expression vectors of RAS proteins were prepared by inserting DNA fragments of corresponding RAS into pRK172-His-TEV-Avi vector. Recombinant RAS proteins were expressed in C41 E. coli (induced with IPTG) followed by AKTA His-trap column. The proteins were further purified by gel filtration using a Superdex 75. Fractions corresponding to RAS

were pooled and concentrated. Protein concentration was determined by Nanodrop. Protein purity and identification was analysed and confirmed by SDS-PAGE stained with Instant Blue and Western blot with corresponding antibodies (figure 17).

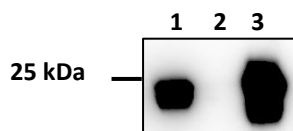
Table 3. A summary of recombinant RAS protein data after purification

Protein	Concentration	Volume
His-TEV-Avi-KRAS166G12V-GppNHp-Biotin	2.8 mg/ml	260ul aliquot X 7
His-TEV-Avi-HRAS-WT-FL-GppNHp-Biotin	0.8 mg/ml	300ul aliquot X 5
His-TEV-Avi-HRAS-WT-FL	3.1 mg/ml	300ul aliquot X 5
His-TEV-Avi-KRAS-WT-FL-GppNHp-Biotin	1.2 mg/ml	300ul aliquot X 9
His-TEV-Avi-KRAS-WT-FL	4.4 mg/ml	300ul aliquot X 16
His-TEV-Avi-NRAS-WT-FL-GppNHp-Biotin	0.9 mg/ml	300ul aliquot X 6
His-TEV-Avi-NRAS-WT-FL	2.8 mg/ml	300ul aliquot X 6

Three wild-type RAS isoforms and their activated conformations were expressed to test the selectivity of compounds. KRASG12V, known as one of the most common KRAS mutations, was expressed to compare the mutant specificity of compounds with KRAS wild-type (figure 17).

a) KRAS

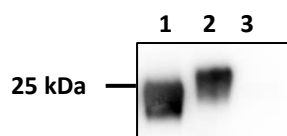
Primary antibody: Anti-KRAS Secondary antibody: Anti-mouse-HRP



1. His-TEV-Avi-KRAS166G12V-GppNHp-Biotin
2. His-TEV-Avi-HRAS166G12V-GppNHp-Biotin (control group)
3. His-TEV-Avi-KRAS-WT-FL

b) HRAS

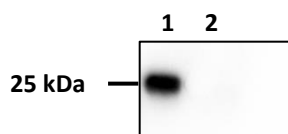
Primary antibody: Anti-HRAS Secondary antibody: Anti-rabbit-HRP



1. His-TEV-Avi-HRAS-GppNHp-Biotin-WT-FL
2. His-TEV-Avi-HRAS-WT-FL
3. His-TEV-Avi-KRAS166G12V-GppNHp-Biotin (control group)

c) NRAS

Secondary antibody: Anti-NRAS Secondary antibody: Anti-goat-HRP



1. His-TEV-Avi-NRAS-WT-FL
2. His-TEV-Avi-KRAS166G12V-GppNHp-Biotin (control group)

Figure 17. Western blot of RAS samples. a) Western blot of KRAS b) Western blot of HRAS c) Western blot of NRAS

Optimization of FP assay

When testing a new FP probe, the first step is to titrate the probe to a certain concentration range in the presence and absence of fixed high concentration RAS protein to determine whether the probe binds to the protein and find the optimal probe concentration for following analysis. In the first FP assay, KRAS166G12V protein in PBS was diluted in 0.02 M HEPES (4-(2-hydroxyethyl)-1-piperazine ethanesulfonic acid), 0.15 M NaCl, 0.5 mM TCEP (tris(2-carboxyethyl)phosphine hydrochloride), 0.05% Tween-20, pH 7.8. As is shown in the graph, an interval of signal strength between FP-RAS-3287-3 probe/RAS protein and the probe alone (referred to as signal window) confirms probe binding. FP signal considerably increased as the probe concentration decreased. An unexpected increase in polarization was observed at high concentration of probe. These responses do not come from spontaneous fluorescence or scattering polarization, but may be non-specific interactions between small molecule aggregates, where hydrophobic parts of the molecules combine to form large micellar particles in an aqueous environment. The biggest signal window was shown between ~3-6 nM probe, which is meaningful in terms of the signal window itself, as higher probe concentrations often lead to low sensitivity, while lower probe concentrations often amplify background noise.

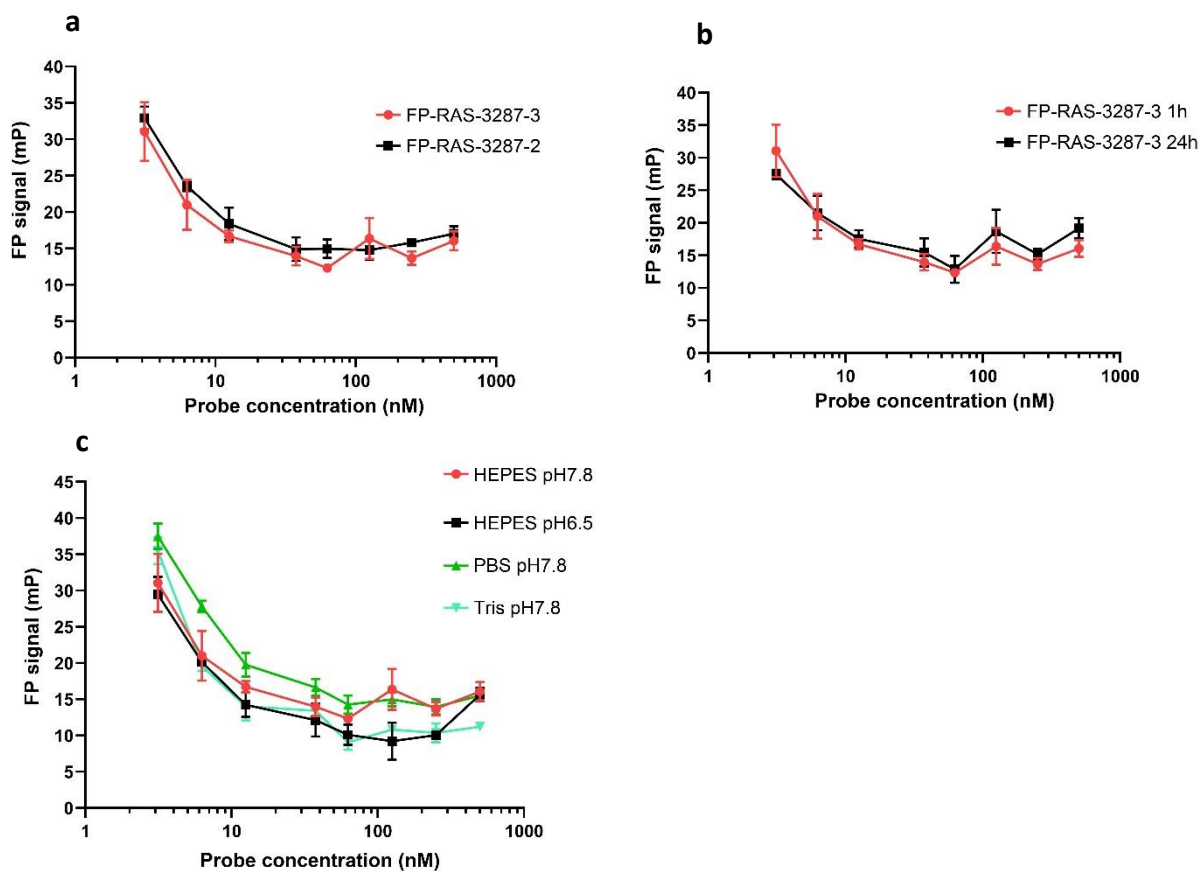


Figure 18. FP values of probe titration. a | Initial FP value of FP-RAS-3287-2 and FP-RAS-3287-3 with increasing concentration in HEPES buffer, pH7.8, 1h b | FP value of FP-RAS-3287-3 increased in 24h c | pH optimization with different pH and buffers

However, the signal is quite narrow (lower than 40 mP) (figure 18a) and not sufficient to measure the binding affinity and stability of protein-probe interaction in the following protein titration experiments. Unfortunately, the similar result was observed on FP-RAS-3287-2. The reasons may be multifaceted, including unoptimized experimental conditions, aggregation or precipitation of the FP probe, weaker binding affinity due to the addition of the fluorophore.

The pH affects both protein ligands binding and the protonation of functional groups in the fluorophores. In order to determine the impact of different pH conditions of buffers on FP binding assay, we selected two common pH values 7.8 and 6.5 in 0.02 M HEPES, 0.15 M NaCl, 0.5 mM TCEP, 0.05% Tween-20, respectively. As shown in figure 18c, the FP assay window did not improve under the environment of pH 6.5, but instead slightly decreased. To determine the impact of different buffer system on FP binding assay, 0.02 M Tris and 0.02 M PBS in 0.15 M NaCl, 0.5 mM TCEP, 0.05% Tween-20, pH7.8 were prepared respectively. It was found that the FP result is clearly influenced by different buffer systems. The performance of FP assay in PBS was improved compared to others, resulting in a maximum change in mP of approximately 6.4 mP, but it was still insufficient for further research. Higher sensitivity was produced by Tris buffer without FP window improvement. This was also discussed by previous FP research. For example, in the study of EZH2-ED interaction inhibitors, it was found that compounds with limited solubility in HEPES (pH 8.0) buffer can be attempted using PIPES (pH 6.2) and Bis-Tris buffer (pH 7.0)¹²⁶. Earlier studies showed that an EZH2-EED interaction inhibitor molecule exhibited severe precipitation and formed aggregates in HEPES buffer¹²⁷. The relatively lower FP values received in Tris buffer system was also mentioned in two other studies^{128, 129}. The study on the optimal time for measuring FP showed that the FP window in most probe concentrations slowly increased until 24 hours, but it did not significantly improve the experimental results to a higher level (figure 18b).

Another issue that may affect fluorescence is solubility and aggregation. Although possible instability was eliminated by structure improvement, the potential solubility issues of FP-RAS probe exposed in HPLC purification was still considered as a serious issue in FP assays. The probe that forms aggregates or precipitates may seriously affect FP values. In this project, 0.05% Tween-20 detergent was applied in FP buffer to help reduce aggregation. However, due to the limited stock of probe samples, solubility is difficult to accurately measure.

This chapter analyses mainly discussed our efforts towards optimization various conditions of FP experiments including assay buffer, pH value, incubation time and detergent. We also evaluated the FP results and discussed different possibilities that FP probe-RAS interaction was impaired. Due to time constraints and experimental material limitations, we were unable

to assess FP conditions with more subdivisions such as other buffer systems (e.g. MES, PIPES) with different pH, temperature, DMSO tolerance and detergents such as Triton™ X-100. However, it is undeniable that the choice of fluorophore and its modification on RAS compounds may have a significant impact on the physicochemical properties and binding affinity. The affinity of the probe may be greatly weakened by the modification of fluorophores and the selection of modification sites. In addition, as mentioned earlier, the solubility of the probe is also questionable. Unfortunately, due to limited material amount, accurate evaluation cannot be achieved. Even through continuous optimization of FP experimental conditions, it may still difficult to achieve a leap in FP window improvement to achieve practical level.

Assay development attempts to validate whether FP probe-RAS interaction is impaired

Fluorescence plate assay

Firstly, we utilized the fluorescence properties inherent in the FP probes attempted to verify the intensity of the interaction between the FP probes and the RAS protein through the characteristics of FP fluorescence itself rather than fluorescence polarization. Referring to the experimental method of enzyme-linked immunosorbent assay (ELISA), the first step was to coat a quantitative HRAS-WT protein (10 ug/ml in 200 ul to each well) on the 96 Well Microplate at 4°C overnight. The plate was washed by PBS and different concentrations of FP probes were added into the well and the plate was incubated for 1h at R.T for probe-RAS binding. Excess unbound probes were washed from the plate and fluorescence intensity signals were measured. Finally, anti-RAS antibody was added to each well and incubated for 1h at R.T, followed by washing with PBS and adding of anti-rabbit-HRP to verify the immobilisation of HRAS protein. BirA was applied as the protein for control group because it

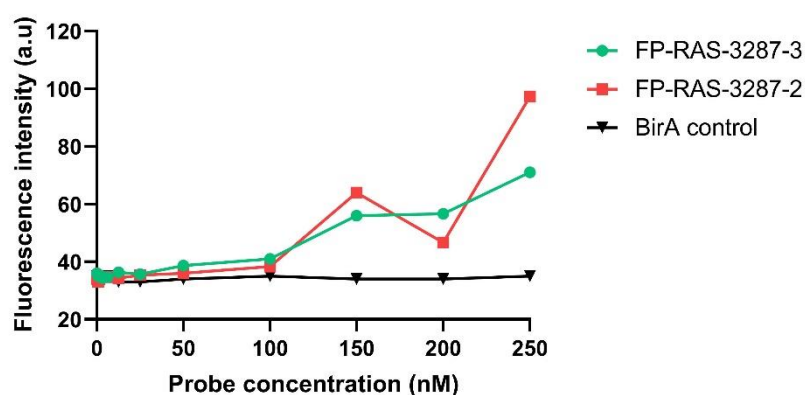


Figure 19. Fluorescence intensity of FP-RAS-3287-2 and FP-RAS-3287-3 with increasing concentration

is a self-prepared protein with good quality and its molecular weight (37.1 kDa) is reasonable compared to HRAS (23.4 kDa).

Figure 19 shows the fluorescence intensity of different groups in the fluorescence plate assay. The stable and identical low fluorescence signal intensity of the BirA control group indicates that the FP probe has specificity in interacting with HRAS proteins, but the threshold sensitivity is low. According to the data, only at high concentrations of FP probes greater than 150 nM, the fluorescence intensity was significantly enhanced compared to the BirA control group. Although considering the possible precipitation or aggregation issues at high probe concentrations, the experimental results positive significance, showing interaction of the FP probe with RAS and therefore that my synthesised FP probe still interacts with RAS protein.

Pull-down assay

Since the FP assay did not give significant outcome, despite the FP probe still interacting with RAS shown by the ELISA assay, my effort was made to develop a new competitive binding high throughput assay for targeting RAS proteins and validate its feasibility and effectiveness. The biotinylated analogue of Ch-3 kindly supplied by John Moses from the Cold Spring Harbour labs, was used in a pull-down assay. Ch-3 shares the same binding site and similar binding mode as the RAS-3287 compound used for FP probe, which can be clearly seen from the X-ray crystal diffraction. KRAS inhibitor BI-2852 mentioned above will be used as a positive control for FP assay and further research. The alignment of crystal structure of BI-2852 and RAS-3287 (figure 7) indicates that BI-2852 is very likely to have significant similarity and competition with RAS-3287 in binding to the same pocket of RAS protein.

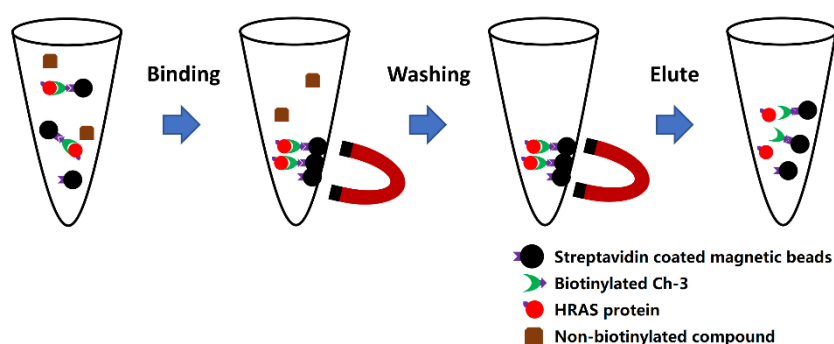


Figure 20. The process of pull-down assay

A mixture of HRAS (0.1 mg/ml; 4.3 μ M) and each non-biotinylated compound (Ch-3, BI-2852 and glutathione) with a certain concentration (107.5 μ M) was incubated individually with increasing concentration of biotinylated Ch-3 compound (53.8 μ M, 107.5 μ M, 215.0 μ M, 430.0 μ M) at 4°C for 1 hour for competition binding. Streptavidin magnetic beads were then added

to immobilize the compound along with the bound RAS protein for 1h. The beads were separated from the solution and washed to obtain both beads and supernatant (solution) (figure 20), followed by anti-His Western blot of beads and supernatant individually.

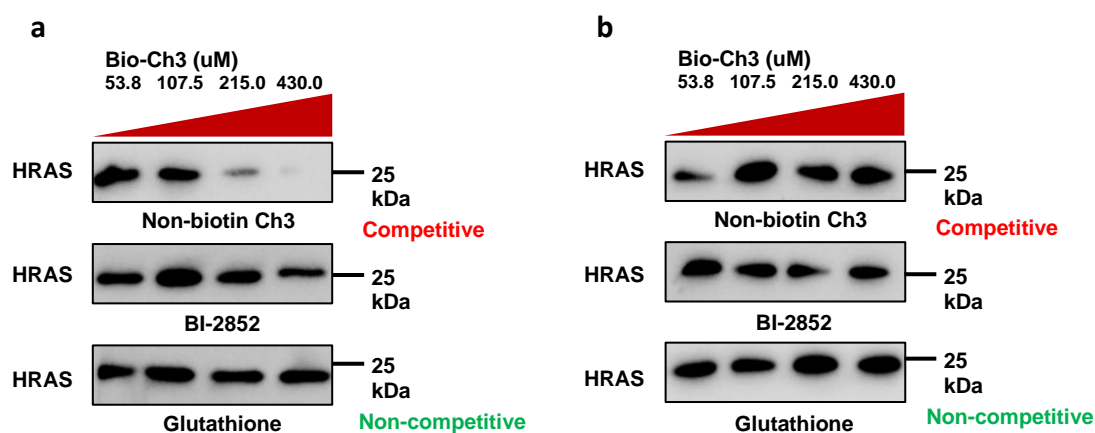


Figure 21. Pull-down Western blot of mixture of HRAS (4.3 uM) + each non-biotinylated compound (Ch-3, BI-2852 and glutathione) (107.5 uM) treated with increasing concentration of biotinylated Ch-3 a| Western blot of supernatant b| Western blot of boiled streptavidin magnetic beads

The Western blot of supernatant seems to better reflect competitive binding than that of beads and subsequent analysis are based on the supernatant Western blot (figure 21). It appears that Ch-3 at a 4X concentration of Non-biotin Ch-3 has almost successfully bound all HRAS proteins and pulled from the solution. In the competitive assay of biotinylated and non-biotinylated Ch-3, it is clear from supernatant Western blot that the band intensity increases with the increase of non-biotinylated concentration. This result also occurs in the Western blot detection of BI-2852 but is not very obvious, which may relate to higher binding affinity or the subtle differences in the binding modes between BI-2852 and Ch/Abd compound series. Compared with BI-2852 and Ch-3, there is no change in band intensity with non-biotinylated compound concentration was observed in the two control groups. The pull-down assay indicates that non-biotinylated compounds may compete with the biotinylated Ch-3 in the RAS-binding state, confirming the feasibility of the pull-down assay in competitive screening of potential RAS protein inhibitors. Competitive pull-down testing provides a valuable and feasible alternative for discovering potential RAS-binding compounds.

Conclusions and future Prospects

This project aims to explore novel RAS-binding compounds based on the understanding and modification of previously identified RAS-compound Abd-7. The Cy5 fluorophore modified Abd-7 was planned as a potential FP probe for RAS-binding study. To achieve this, the compound structure was redesigned with benzylamine/ phenethylamine to adapt to addition

of fluorophore Cy5. Two FP compounds with different structure were successfully developed by *de novo* synthesis. It was found that both compounds showed binding with RAS in FP assay but did not provide sufficient FP signal windows for subsequent biochemical research due to various possible reasons including exceptionally poor solubility of the probes, setting of assay conditions, aggregation or precipitation, weaker binding affinity caused by FP modification. The optimization of FP assay conditions did not significantly improve the signal window. A plate assay similar to ELISA was developed to validate whether FP probe-RAS interaction was severely influenced. It shows that the probe exhibits strong signal at high concentrations, which confirms the hypothesis. We used biotinylated Ch-3 with the same binding site as Abd-7 to establish a competitive pull-down assay, seeking a new way to identify and evaluate small molecules interacting with RAS. The results confirmed the feasibility of pull-down analysis in competitive screening of potential RAS protein inhibitors. It also provides a potential alternative for discovering RAS-binding compounds, such as the possibility of high-throughput development by adopting 96 well plates, ELISA/BCA protein assay.

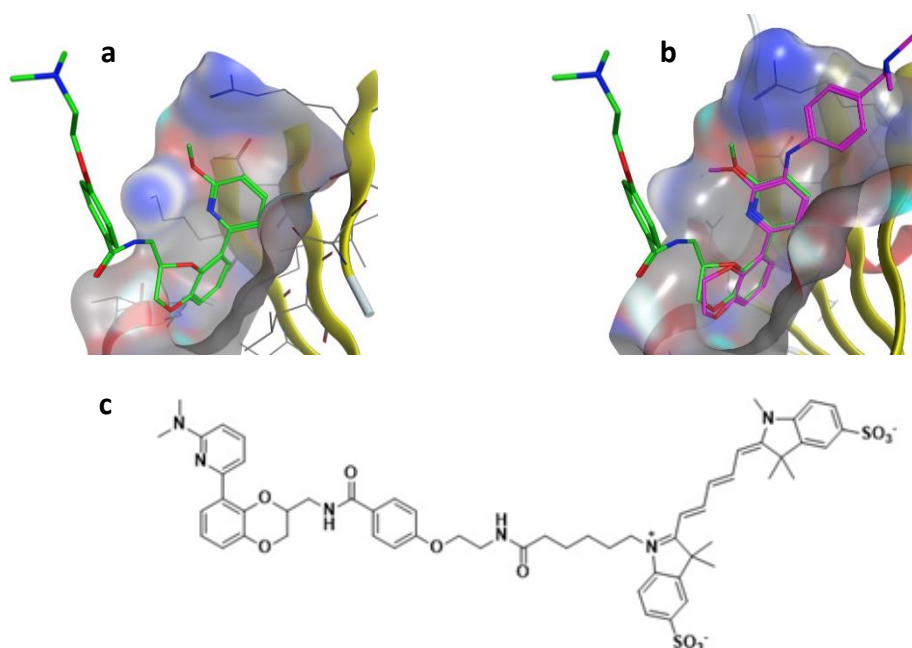


Figure 22. High resolution crystal structure shows how RAS-3162 and RAS-3287 compounds bind to the same KRASG12D pocket. a) RAS-binding compound 3162 (PDB: 6FA2) b) Alignment of RAS-3162 (green) (PDB: 6FA2) and RAS-3287 (violet) (PDB: 6FA4) c) Structure of proposed FP-RAS-3162 with Sulfo-Cy5 fluorophore

Although the general method for designing fluorescent probe is based on modification of molecules with known pharmacological properties, the result of FP assay is sometimes elusive and unpredictable. Due to time constraints, material factors, and research institutions, there are some technologies that were not applied in this project, and there is also room for further exploration and optimization in experimental design and assay conditions. In this project, the

modification of the fluorescent group of the compound may lead to changes in the physical and biochemical properties of the compound. In terms of probe structure design, other sites or analogues with same binding site (e.g. RAS-3162 in figure 22) can be considered for further modification, and more different types (fluorescein, rhodamine, cyanine, etc.) or emission wavelength of fluorophores can be attempted. The FP assay conditions can also be further explored by evaluating the influence of different buffers (e.g. MES, PIPES), pH, temperatures, and detergents (e.g. Triton™ X-100) on the results to seek a larger FP window.

Other techniques can also be applied to examine the interaction between probes and proteins. SPR has good sensitivity and small sample consumption, which is very conducive to preliminary testing binding of FP probes. For crystallizable proteins such as RAS, X-ray diffraction provides an indication of the three-dimensional structure of a material, which helps understand the structure–activity relationship of FP probes and further improvement of probe design. Other techniques such as ITC, waterLOGSY would be considered as feasible alternatives.

In addition, considering the possible optical interference from compound autofluorescence or precision, an improved solution for current FP probe is to convert the FP assay to a TR-FRET format using terbium labelled antibody. By utilizing the emission peak of terbium to overlap with the excitation spectrum of the FP fluorophore, terbium is used as the FRET donor and the fluorophore as the receptor, which improves sensitivity and reduces interference.

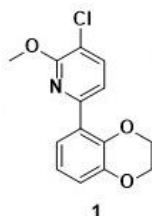
Experimental

General Synthetic Chemistry

Unless otherwise noted, all the chemistry reactions were carried out in oven-dried clean glassware under an atmosphere of inert N₂ atmosphere at stated temperature. Normal phase chromatography was conducted on Biotage® SNAP KP-Sil prepacded silica cartridges. Reverse phase chromatography was carried out on Biotage® SNAP ultra C18 cartridges. Ion-exchange chromatography was performed using ISOLUTE Flash SCX-2 cartridges. Analytical TLC was carried out on aluminum backed TLC plates with silica gel coated with UVP Mini UV Viewing Cabinets (observed under 254/365 nm UV). ¹H and ¹³C NMR spectra were measured at room temperature with a Bruker AV500a/AV500b/AV600 spectrometer at 500/600 MHz and 126 MHz respectively. Chemical shifts (δ) were recorded in parts per million (ppm), corrected by solvent residue peak. Coupling constants (J) were measured in Hertz (Hz). ¹H NMR data is written with format: chemical shift, multiplicity, J coupling and integration. ¹³C NMR data is written with format: chemical shift. The multiplicities are marked by following abbreviations: s

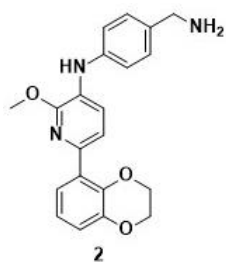
for singlet; d for doublet; t for triplet; m for multiplet. IR spectroscopy was measured by Agilent Cary 630 FTIR spectrometer. Mass spectrometry was measured by Medicinal Chemistry 4 Team (including Analytical Chemistry) of the Institute of Cancer Research. LC-MS was detected by Agilent 1200 Series Prep Scale diode array detector with a 6210 time-of-flight (ToF) mass spectrometer (Phenomenex Kinetex C18 column, 30 x 2.1 mm, 2.6u, 100A, flow rate of 0.4 ml/min in a 4 minute gradient elution at 40 °C with detection at 254, 280 and 214 nm) or Waters Acquity UPLC detector with Waters Xevo G2QToF mass spectrometer (Agilent Poroshell C18 column, 30 x 2.1 mm, 2.6u, flow rate of 0.3 ml/min in a 4 min gradient elution at 30 °C with detection at 254 nm), with ionisation by positive-ion electrospray (ESI⁺). The mobile phase of Agilent QToF2 was a mixture of methanol (solvent A) and water (solvent B), both containing formic acid at 0.1%. Gradient elution was as follows: 10:90 (A/B) to 90:10 (A/B) over 2.5 min, 90:10 (A/B) for 1 min, and then reversion back to 10:90 (A/B) over 0.3 min, finally 10:90 (A/B) for 0.2 min. The mobile phase of Waters Xevo was a mixture of methanol (solvent A) and water (solvent B), both containing formic acid at 0.1%. Gradient elution was as follows: 10:90 (A/B) to 90:10 (A/B) over 3 min, 90:10 (A/B) for 0.5 min, and then reversion back to 10:90 (A/B) over 0.3 min, finally 10:90 (A/B) for 0.2 min. Compound purity was assessed by UV absorbance at 254 nm.

3-Chloro-6-(2,3-dihydrobenzo[b][1,4]dioxin-5-yl)-2-methoxypyridine 1



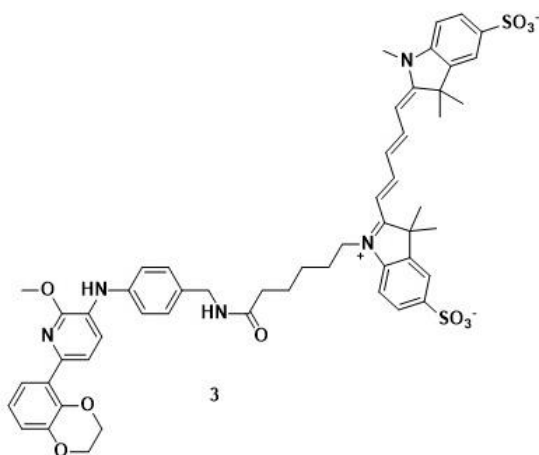
2-(2,3-Dihydro-1,4-benzodioxin-5-yl)-4,4,5,5-tetramethyl-1,3,2-dioxaborolane (250 mg, 0.95 mmol), 6-bromo-3-chloro-2-methoxypyridine (233 mg, 1.05 mmol) and potassium carbonate (264 mg, 1.91 mmol) were added to a solution of 1,4-dioxane (5.8 ml) and water (0.58 ml) with N₂ protection in a 5 ml microwave vial. Tetrakis (triphenylphosphine) palladium (0) (56 mg, 0.05 mmol) was added and purged for 5 min with N₂. The reaction mixture was then sealed and heated for 2 hours at 110 °C. The reaction was concentrated under reduced pressure, re-dissolved in EtOAc, washed with water (20 ml) and brine (20 ml). The organic phase was dried over MgSO₄, purified by Biotage® silica chromatography (Sfär 10 g, EtOAc/cyclohexane 0-40%, 2CV, gradient over 15 CV, 5 CV) and concentrated under reduced pressure to obtain the title compound (155 mg, 59%, 0.56 mmol). ¹H NMR (500 MHz, CDCl₃) δ 7.63 (d, J = 8.0 Hz, 1H), 7.52 (dd, J = 7.0, 2.5 Hz, 1H), 7.50 (d, J = 8.0 Hz, 1H), 6.99 – 6.88 (m, 2H), 4.38 – 4.26 (m, 4H), 4.09 (s, 3H). ¹³C NMR (126 MHz, CDCl₃) δ 158.6, 150.3, 144.1, 141.9, 138.2, 128.0, 123.0, 121.2, 118.7, 118.1, 116.4, 64.5, 64.2, 54.2. MS (ESI⁺) m/z 278, 92% (M+H)⁺.

N-(4-(Aminomethyl)phenyl)-6-(2,3-dihydrobenzo[b][1,4]dioxin-5-yl)-2-methoxypyridin-3-amine 2



To a solution of 3-chloro-6-(2,3-dihydro-1,4-benzodioxin-5-yl)-2-methoxy-pyridine (40 mg, 0.14 mmol) in 1,4 dioxane (1.4 ml) was added 4-[(N-Boc)aminomethyl]aniline (32 mg, 0.14 mmol), sodium tert-butoxide (21 mg, 0.22 mmol) and XPhos Pd(crotyl)Cl (9.7 mg, 0.014 mmol). The reaction was degassed with N₂ for 5 min, heated at 100 °C for 19 h and then cooled down to room temperature. 4 M HCl in dioxane (0.72 ml) was added to the reaction mixture and stirred at room temperature for 2.5 h. The mixture was loaded to SCX-2 2g column, washed with MeOH and eluted with 1M ammonia in MeOH. The elution was concentrated under reduced pressure, purified by reverse phase chromatography Snap C18 ultra 12 g (0-100% MeOH in water, 0.1% formic acid, 2 CV, gradient over 15 CV, 5 CV) and re-concentrated under reduced pressure to obtain the title compound (30 mg, 57%, 0.08 mmol). ¹H NMR (500 MHz, CDCl₃) δ 8.32 (s, 1H), 7.50 (dd, J = 7.7, 1.8 Hz, 1H), 7.42 (d, J = 8.0 Hz, 1H), 7.38 (d, J = 8.1 Hz, 1H), 7.24 (s, 2H), 7.03 (d, J = 8.0 Hz, 2H), 6.89 (t, J = 7.9 Hz, 1H), 6.83 (dd, J = 8.0, 1.8 Hz, 1H), 4.24 (s, 4H), 3.99 (s, 3H), 3.85 (s, 2H). MS (ESI⁺) m/z 364, 100% (M+H)⁺.

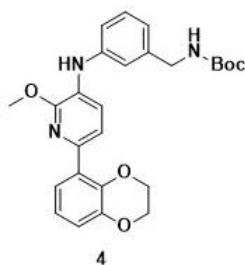
1-(6-((4-((6-(2,3-Dihydrobenzo[b][1,4]dioxin-5-yl)-2-methoxypyridin-3-yl)amino)benzyl)amino)-6-oxohexyl)-3,3-dimethyl-2-((1E,3E)-5-((E)-1,3,3-trimethyl-5-sulfonatoindolin-2-ylidene)penta-1,3-dien-1-yl)-3H-indol-1-ium-5-sulfonate 3



Reaction carried out in a micro LC-MS vial with N-[4-(aminomethyl)phenyl]-6-(2,3-dihydro-1,4-

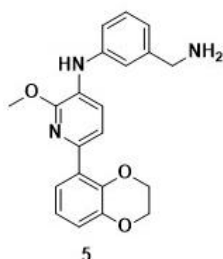
benzodioxin-5-yl)-2-methoxy-pyridin-3-amine (0.70 mg, 0.0019 mmol). Sodium 1-(6-((2,5-dioxopyrrolidin-1-yl)oxy)-6-oxohexyl)-3,3-dimethyl-2-((1E,3E)-5-((E)-1,3,3-trimethyl-5-sulfonatoindolin-2-ylidene)penta-1,3-dien-1-yl)-3H-indol-1-ium-5-sulfonate (1.00 mg, 0.0013 mmol) dissolved using 200 ul of a triethylamine (20 ul) in DMF (300 ul) was added. The reaction mixture was dissolved on vortex shaker, shielded from artificial light and stood for 16 hours. The title compound was detected by LC-MS. MS (ESI⁺) m/z 1010, 48% (M+H)⁺. The mixture was then loaded onto standard 5 ml/min lipophilic HPLC semi-prep set to collect all. Artificial lights were turned off as best as possible and evaporation bath was covered with foil. Desired fractions were combined and concentrated under reduced pressure. No UV/MS peak of objective compound was observed in any HPLC fractions.

Tert-Butyl (3-((6-(2,3-dihydrobenzo[b][1,4]dioxin-5-yl)-2-methoxypyridin-3-yl)amino)benzyl)carbamate 4



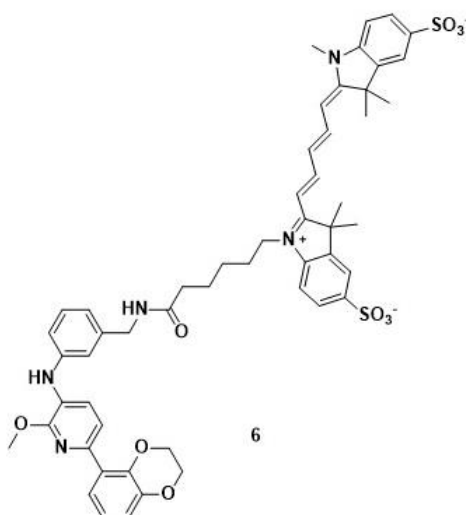
To a solution of 3-chloro-6-(2,3-dihydro-1,4-benzodioxin-5-yl)-2-methoxy-pyridine (112 mg, 0.40 mmol) in 1,4 dioxane (5.0 ml) was added tert-butyl 3-aminobenzylcarbamate (99 mg, 0.45 mmol) and sodium tert-butoxide (58 mg, 0.61 mmol). The reaction mixture was degassed with N₂ for 5 min and heated at 100 °C for 4 h. The reaction mixture was diluted by EtOAc (10 ml) and washed with brine (2 x 20 ml). The organic layer was dried over Na₂SO₄ and concentrated under reduced pressure. The mixture was purified by Biotage® normal phase chromatography (Sfär 10 g EtOAc/cyclohexane 0-30%, 2CV, gradient over 15 CV, 5 CV) and concentrated under reduced pressure to obtain the title compound (155 mg, 83%, 0.33 mmol). ¹H NMR (500 MHz, CDCl₃) δ 7.53 (dd, J = 7.7, 1.7 Hz, 1H), 7.51 – 7.46 (m, 2H), 7.32 – 7.23 (m, 1H), 7.11 – 7.06 (m, 2H), 6.94 – 6.88 (m, 3H), 6.86 (dd, J = 8.0, 1.7 Hz, 1H), 4.32 (dddd, J = 10.1, 8.3, 5.0, 3.4 Hz, 7H), 4.12 (s, 3H), 1.47 (s, 9H). MS (ESI⁺) m/z 464, 100% (M+H)⁺.

N-(3-(Aminomethyl)phenyl)-6-(2,3-dihydrobenzo[b][1,4]dioxin-5-yl)-2-methoxypyridin-3-amine 5



To a solution of tert-butyl N-[[3-[[6-(2,3-dihydro-1,4-benzodioxin-5-yl)-2-methoxy-3-pyridyl]amino]phenyl]methyl]carbamate (40 mg, 0.09 mmol) in MeOH (0.43 ml) was added 4M HCl in 1,4-dioxane (0.43 ml, 1.73 mmol). The mixture was stirred at room temperature for 1.5 h, purified by SCX column (1 g) and concentrated under reduced pressure to obtain the title compound (23 mg, 74%, 0.06 mmol). ¹H NMR (500 MHz, CDCl₃) δ 7.55 (dd, J = 7.7, 1.7 Hz, 1H), 7.50 (s, 2H), 7.29 – 7.23 (m, 1H), 7.12 (d, J = 1.9 Hz, 1H), 7.06 (dd, J = 8.1, 2.2 Hz, 1H), 6.97 – 6.89 (m, 2H), 6.85 (dd, J = 8.0, 1.8 Hz, 1H), 6.22 (s, 1H), 4.37 – 4.27 (m, 4H), 4.08 (s, 3H), 3.85 (s, 2H). ¹³C NMR (126 MHz, CDCl₃) δ 152.6, 144.1, 144.0, 142.1, 141.5, 141.3, 129.7, 129.0, 126.6, 122.6, 121.0, 120.6, 119.4, 118.2, 117.6, 117.3, 116.7, 64.5, 64.2, 53.5, 46.3. MS (ESI⁺) m/z 364, 100% (M+H)⁺.

1-(6-((3-((6-(2,3-Dihydrobenzo[b][1,4]dioxin-5-yl)-2-methoxypyridin-3-yl)amino)benzyl)amino)-6-oxohexyl)-3,3-dimethyl-2-((1E,3E)-5-((E)-1,3,3-trimethyl-5-sulfonatoindolin-2-ylidene)penta-1,3-dien-1-yl)-3H-indol-1-ium-5-sulfonate 6

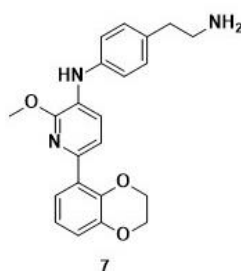


Reaction carried out in a micro LC-MS vial with N-[3-(aminomethyl)phenyl]-6-(2,3-dihydro-1,4-benzodioxin-5-yl)-2-methoxy-pyridin-3-amine (0.65 mg, 0.0018 mmol). Sodium 1-(6-((2,5-dioxopyrrolidin-1-yl)oxy)-6-oxohexyl)-3,3-dimethyl-2-((1E,3E)-5-((E)-1,3,3-trimethyl-5-sulfonatoindolin-2-ylidene)penta-1,3-dien-1-yl)-3H-indol-1-ium-5-sulfonate (1.00 mg, 0.0013

mmol) dissolved using 200 ul of a triethylamine (20 ul) in DMF (300 ul) was added. The reaction mixture was dissolved on vortex shaker, shielded from artificial light and stood for 17 hours. The title compound was detected by LC-MS. MS (ESI⁺) m/z 988, 72% (M+H)⁺. The mixture was then loaded onto HPLC semi-prep set to collect all. Artificial lights were turned off as best as possible and evaporation bath was covered with foil. Desired fractions were combined and concentrated under reduced pressure. No UV/MS peak of objective compound was observed in any HPLC fractions.

The reaction was improved and conducted by Dr. John Caldwell. Sodium 1-(6-((2,5-dioxopyrrolidin-1-yl)oxy)-6-oxohexyl)-3,3-dimethyl-2-((1E,3E)-5-((E)-1,3,3-trimethyl-5-sulfonatoindolin-2-ylidene)penta-1,3-dien-1-yl)-3H-indol-1-ium-5-sulfonate (1.07 mg) was added to a brown glass LC-MS vial. N-[3-(aminomethyl)phenyl]-6-(2,3-dihydro-1,4-benzodioxin-5-yl)-2-methoxy-pyridin-3-amine (0.77 mg, 0.0021 mmol), DMF (26.25 uL, 0.05 M) and triethylamine (0.96 uL, 0.007 mmol) were added to the vial separately. The reaction mixture was stirred on vortex shaker, shielded from artificial light and stood for 19 h. The reaction mixture was dilute with a further 170 uL of DMF and purified through column Biotage® Sfär C18 6 g (0-100% MeOH in water, 0.1% formic, 2 CV, gradient over 20 CV, 5 CV), loading with 0.4 mL of DMSO. The desired fractions were dissolved in methanol and purified through a 500 mg SCX-2 column with methanol to give the title compound (1.09 mg, 79%, 0.0011 mmol). MS (ESI⁺) m/z 988, 100% (M+H)⁺.

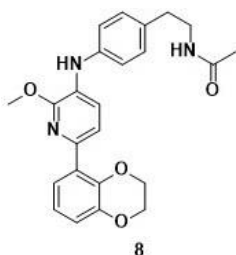
N-(4-(2-Aminoethyl)phenyl)-6-(2,3-dihydrobenzo[b][1,4]dioxin-5-yl)-2-methoxypyridin-3-amine 7



To a solution of 3-chloro-6-(2,3-dihydro-1,4-benzodioxin-5-yl)-2-methoxy-pyridine (48 mg, 0.17 mmol) in 1,4 dioxane (2.2 mL) was added tert-butyl N-[2-(4-aminophenyl)ethyl]carbamate (45 mg, 0.19 mmol) and Sodium tert-butoxide (25 mg, 0.26 mmol) . The reaction mixture was degassed with N₂ for 5 min, heated at 100 °C for 3.5h. The reaction mixture was diluted by EtOAc (10 ml) and washed with brine (2 x 20 ml). The organic layer was dried with Na₂SO₄ and concentrated under reduced pressure. The crude product was purified by Biotage® normal phase chromatography (Sfär 10 g Ethyl acetate/cyclohexane 0-30%, 2CV, gradient over 15 CV, 5 CV) and concentrated to obtain the title compound (57 mg, 88%, 0.15 mmol).

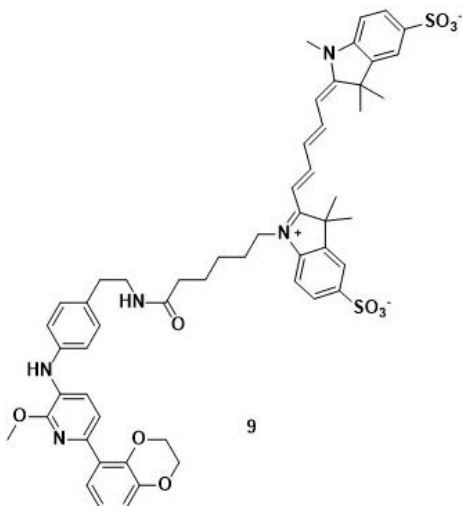
^1H NMR (600 MHz, CDCl_3) δ 7.53 (dd, $J = 7.8, 1.7$ Hz, 1H), 7.48 – 7.40 (m, 2H), 7.16 – 7.09 (m, 4H), 6.92 (t, $J = 7.9$ Hz, 1H), 6.84 (dd, $J = 8.0, 1.7$ Hz, 1H), 6.13 (s, 1H), 4.30 (ddt, $J = 8.7, 7.0, 2.5$ Hz, 4H), 4.08 (s, 3H), 2.98 (t, $J = 7.0$ Hz, 2H), 2.74 (t, $J = 6.9$ Hz, 2H). ^{13}C NMR (151 MHz, CDCl_3) δ 152.4, 144.0, 141.5, 140.8, 139.9, 133.3, 129.9, 129.1, 127.2, 122.6, 121.1, 119.6, 119.5, 118.6, 118.2, 116.7, 77.4, 77.2, 76.9, 64.5, 64.2, 53.5, 43.6, 39.0. MS (ESI $^+$) m/z 378, 100% (M+H) $^+$.

N-(4-((6-(2,3-Dihydrobenzo[b][1,4]dioxin-5-yl)-2-methoxypyridin-3-yl)amino)phenethyl)acetamide 8



Reaction carried out in a micro LC-MS vial with N-[4-(2-aminoethyl)phenyl]-6-(2,3-dihydro-1,4-benzodioxin-5-yl)-2-methoxy-pyridin-3-amine (1.0 mg, 0.0026 mmol) and 2,5-Dioxopyrrolidin-1-yl acetate (0.54 mg, 0.0034 mmol) dissolved using 200 μl of a triethylamine (20 μl) in DMF (300 μl). The vial was stood for 5 days. The mixture was then loaded onto HPLC semi-prep set to collect all. Artificial lights were turned off as best as possible and evaporation bath was covered with foil. Desired fractions were combined and concentrated under reduced pressure to obtain the title compound. MS (ESI $^+$) m/z 420, 100% (M+H) $^+$.

1-(6-((4-((6-(2,3-Dihydrobenzo[b][1,4]dioxin-5-yl)-2-methoxypyridin-3-yl)amino)phenethyl)amino)-6-oxohexyl)-3,3-dimethyl-2-((1E,3E)-5-((E)-1,3,3-trimethyl-5-sulfonatoindolin-2-ylidene)penta-1,3-dien-1-yl)-3H-indol-1-ium-5-sulfonate 9



Reaction carried out in a micro LC-MS vial. N-[4-(2-aminoethyl)phenyl]-6-(2,3-dihydro-1,4-benzodioxin-5-yl)-2-methoxy-pyridin-3-amine (0.64 mg, 0.0017 mmol) in vial. Add sodium 1-(6-((2,5-dioxopyrrolidin-1-yl)oxy)-6-oxohexyl)-3,3-dimethyl-2-((1E,3E)-5-((E)-1,3,3-trimethyl-5-sulfonatoindolin-2-ylidene)penta-1,3-dien-1-yl)-3H-indol-1-ium-5-sulfonate (1.00 mg, 0.0013 mmol) dissolved using 200 uL of a 20 uL triethylamine in 300 uL of DMF. Dissolve on vortex shaker, shield from artificial light and stand deep blue solution for 41 hours. XV22_00131 showed peak at 1.49 min, 1002 mass ion. Load onto standard 5 mL/min lipophilic HPLC semiprep set to collect all (0.5 min fractions). Turn artificial lights off on sample collection and injection wells. The sample was injected in HPLC with 2 x extended gradient elution (40% to 100% MeOH) and 2 x washing (100% MeOH). Desired fractions were combined, concentrated to obtain the title compound (1.24 mg, 94%, 0.0012 mmol). ¹H NMR (600 MHz, MeOD) δ 8.24 (td, J = 13.1, 3.8 Hz, 2H), 7.91 – 7.85 (m, 4H), 7.49 – 7.40 (m, 3H), 7.28 (dd, J = 13.9, 8.5 Hz, 2H), 7.18 – 7.09 (m, 4H), 6.83 (t, J = 7.9 Hz, 1H), 6.76 (dd, J = 8.0, 1.7 Hz, 1H), 6.57 (t, J = 12.4 Hz, 1H), 6.25 (d, J = 13.7 Hz, 1H), 6.19 (d, J = 13.7 Hz, 1H), 4.26 (s, 4H), 4.04 (t, J = 7.5 Hz, 2H), 3.99 (s, 3H), 3.55 (s, 3H), 3.42 (t, J = 7.1 Hz, 2H), 2.74 (t, J = 7.1 Hz, 2H), 2.17 (t, J = 7.1 Hz, 2H), 1.76 (p, J = 7.7 Hz, 2H), 1.71 (d, J = 3.3 Hz, 12H), 1.64 (p, J = 7.2 Hz, 2H), 1.47 – 1.30 (m, 2H). ¹³C NMR (151 MHz, MeOD) δ 176.0, 175.7, 175.2, 173.0, 156.2, 153.9, 145.5, 145.4, 144.8, 143.5, 142.6, 142.5, 142.2, 141.8, 133.5, 130.8, 130.0, 128.4, 128.1, 127.7, 123.3, 121.6, 121.4, 121.2, 120.1, 120.0, 119.1, 117.5, 111.6, 111.4, 105.3, 105.1, 65.6, 65.3, 61.5, 53.8, 50.6, 45.0, 41.7, 36.7, 35.9, 30.8, 28.1, 27.8, 27.7, 27.1, 26.4, 20.9, 14.5. MS (ESI⁺) m/z 1002, 100% (M+H)⁺.

Expression and purification of RAS proteins

DNA fragments of corresponding RAS were inserted into pRK172-His-TEV-Avi vector to make expression vectors. The plasmids were transformed into *E. coli* C41(DE3). Bacterial cells were cultured at 37 °C to an OD₆₀₀ of 0.5 and induced with 0.5 mM IPTG (isopropyl 1-thio-beta-D-galactopyranoside) at 16 °C, 225 rpm overnight. The bacteria cultures were harvested by centrifugation at 4000 rpm for 20 min and the cell pellets were re-suspended in lithium borate (LB) buffer. The proteins were extracted by cell disruptor (Constant Systems Ltd., UK) at 25,000 psi at 4 °C and resuspended in Buffer A (50 mM HEPES, pH 7.4, 500 mM NaCl, 5% glycerol, 20 mM imidazole) with protease inhibitor (Sigma, P8340) and kept on ice. The proteins were purified using His-Trap Ni-affinity columns (GE Healthcare, 17-5248-02) employing gradient elution (20-300 mM imidazole) and concentrated using pro affinity concentrator (Amicon). The proteins were further purified by size exclusion chromatography on a HiLoad Superdex-75 HR column (GE Healthcare) in PBS, pH 7.4, 5 mM MgCl₂ and reconcentrated for storage at -80 °C.

GTP Loading

The RAS proteins were concentrated/diluted to approximately 2 mg/ml. RAS protein solution (500 μ l, 2 mg/ml), GppNHp (7.5 μ l, 100 mM), 10x alkaline phosphatase buffer (100 μ l), water (up to 1ml) and Alkaline phosphatase (1 μ l, 30 U/ml) were added in 1ml Eppendorf. The mixture was incubated at room temperature for 2 h and inactivated by adding 50 μ l of 1M MgCl₂.

Biotinylation

The solution of RAS proteins (1 ml) were incubated with 10 μ l BirA (7.5 mg/ml), MgCl₂ (5 μ l, 1M), biotin (10 μ l, 50 mM in DMSO) and ATP (20 μ l, 100 mM) at 4 °C overnight. Biotinylation of RAS proteins was determined by adding 5 μ l streptavidin agarose pre-washed with PBS, pH 7.4, 5 mM MgCl₂ to 30 μ l RAS solution. The mixture was incubated at room temperature for 30 min with slow rotation and centrifuged at 4000 rpm for 1 min. The samples of the flow through and beads were analysed by Coomassie blue staining of SDS-PAGE.

Western blot

95 μ l of Milli-Q water and add 25 μ l of 5x loading buffer (each 10 ml contained: 1.75 ml of 0.5 M Tris-Cl pH 6.8, 4.5 ml glycerol, 0.5 g SDS, 25 mg bromophenol blue, 1.25 ml BME) were added to 5 μ l of RAS solutions (1 mg/ml). The samples were heated at 95 °C for 6 minutes and fractionated on 15% SDS-PAGE. The gel underwent electrophoresis at 140V for 90 min and transferred to polyvinylidene fluoride (PVDF) membrane (GE Healthcare). The membrane was blocked with 10% non-fat milk (Sigma) in TBS-0.1% Tween20 and incubated overnight at 4°C. The membrane was incubated for 1.5 h at room temperature with appropriate primary and secondary antibodies separately. Primary antibodies included anti-His-HRP (1/2000, Sigma, A7058), anti-pan-RAS (1/200, Millipore, OP40), anti-HRAS (1/500, Proteintech, 18295-1-AP), anti-KRAS (1/100, Santa Cruz Biotechnologies, sc-30) and anti-NRAS (1/100, Santa Cruz Biotechnologies, sc-31). Secondary antibodies included anti-mouse-HRP (CST, 7076), anti-goat-HRP (Santa Cruz Biotechnologies, 2354) and anti-rabbit-HRP (CST, 7074). The membranes were washed with TBS-0.1% Tween for 1 h and visualized using Clarity Western ECL Substrate (Bio-Rad) and ChemiDoc XRS+ imaging system (Bio-Rad).

FP assay

Unless otherwise stated the aqueous assay buffer contained 0.02 M HEPES pH 7.8 0.15 M NaCl, 0.5 mM TCEP, 0.05% Tween-20. The assay was conducted using 384 well black Proxi plates (Perkin-Elmer) with a final assay volume of 10 μ l. Plates were centrifuged at 1000 rpm

for 1 minute and incubated for 1h. Plates were read using a PHERAstar FSX Microplate Reader (BMG LABTECH) with FP optic module 590-50/675-50/675-50. Excitation and emission wavelengths used for green probes were 480 nm and 535 nm, respectively. Fluorescence polarization was measured in units of millipolarization (mP) and all experiments were performed in triplicate unless otherwise stated.

Plate assay

Wells of black 96-well maxisorp plate (Thermo Scientific™, 437111) were coated with 10ug/ml of His-TEV-Avi-HRAS-WT-FL protein (200 ul per well) at 4°C overnight. The plate was washed 3 times with PBS containing 0.05% Tween-20 and each well was blocked with 250 ul 5% BSA in PBS for 4 h at R.T. The plate was then washed 2 times with PBS followed by addition of 100 ul FP probe with different concentration to bind for 1 h at R.T. The plate wells were washed 3 times with 300 ul PBS by multichannel pipette. The fluorescence was measured using a PHERAstar FSX Microplate Reader (BMG LABTECH). 200 ul of anti-pan-RAS (1/200, Millipore, OP40) (1:1000) was added to each well and incubated for 1h at R.T. The plate was washed by PBS with 0.05% Tween-20 and 250 ul of anti-rabbit-HRP (CST, 7074) (1:1000) was added to each well and incubated for 30min at R.T., followed by 3 times washing with PBS containing 0.05% Tween-20. 250ul of PBS was added to each well and the fluorescence was measured using a PHERAstar FSX Microplate Reader (BMG LABTECH).

Pull-down assay with biotinylated Ch-3

Mixture at molar ratio of 1 His-TEV-Avi-HRAS-WT-FL protein (0.1 mg/ml; 4.3 uM) : 25 one of non-biotinylated compounds (Ch-3, BI-2852 (Boehringer Ingelheim), glutathione) (107.5 uM) was incubated with increasing concentration (12.5, 25, 50, 100 times with His-TEV-Avi HRAS) of biotinylated Ch-3 and made to 50 ul of PBS, pH 7.4 individually at 4°C for 1 hour. The Pierce™ Streptavidin Magnetic Beads (Thermo Scientific™, 88816) were incubated with BSA (21.5 uM) at 4°C for 30 min. The beads were then washed 3 times with PBS and resuspended in PBS. 50 ul of beads was added to each sample with gentle agitation and incubated with the mixture at 4°C for 1h. The beads were separated from the solution by DynaMag™-2 Magnet (Thermo) and washed 2 times with PBS to remove excess unbound biotinylated Ch-3, followed by anti-His Western blot of beads and supernatant individually.

ACKNOWLEDGMENTS

I would like to express my deepest appreciation to Prof. Terry Rabbits, Dr. John Caldwell and Prof. Ian Collins for their patient guidance and support throughout the project. Moreover, I am grateful to Dr. Amal J Sivaram, Dr. Nikki Sereesongaeng and Mrs. Iona Black for their useful

comments and suggestions. A special gratitude goes to Dr. Mark Stubbs, Dr. Amin Mirza, Dr Maggie Liu, Mr. Joe Smith and Prof. John Moses for their generous help in technical assistance.

References

1. Colicelli, J., Human RAS superfamily proteins and related GTPases. *Science's STKE* **2004**, 2004 (250), re13-re13.
2. Zinatizadeh, M. R.; Masoumalinejad, Z.; Parnak, F., The prevalence of Mycoplasma hyorhinis contamination in tissues samples from cancer patients: A Brief Report. *Modern Medical Laboratory Journal* **2018**, 2 (1), 91-95.
3. Erickson, K. E.; Rukhlenko, O. S.; Posner, R. G.; Hlavacek, W. S.; Kholodenko, B. N. In *New insights into RAS biology reinvigorate interest in mathematical modeling of RAS signaling*, Seminars in cancer biology, Elsevier: 2019; pp 162-173.
4. Bartoš, F., Histotopochemistry of Ascorbic Acid in Tendon Fibres. *Nature* **1964**, 204 (4963), 1104-1104.
5. Kirsten, W.; Mayer, L., Malignant lymphomas of extrathymic origin induced in rats by murine erythroblastosis virus. *Journal of the National Cancer Institute* **1969**, 43 (3), 735-746.
6. Clark, L. L.; Ingall, E. D.; Benner, R., Marine phosphorus is selectively remineralized. *Nature* **1998**, 393 (6684), 426-426.
7. Johnson, L.; Greenbaum, D.; Cichowski, K.; Mercer, K.; Murphy, E.; Schmitt, E.; Bronson, R. T.; Umanoff, H.; Edelman, W.; Kucherlapati, R., K-ras is an essential gene in the mouse with partial functional overlap with N-ras. *Genes & development* **1997**, 11 (19), 2468-2481.
8. Campbell, S. L.; Khosravi-Far, R.; Rossman, K. L.; Clark, G. J.; Der, C. J., Increasing complexity of Ras signaling. *Oncogene* **1998**, 17 (11), 1395-1413.
9. Neal, S. E.; Eccleston, J. F.; Hall, A.; Webb, M. R., Kinetic analysis of the hydrolysis of GTP by p21N-ras. The basal GTPase mechanism. *Journal of Biological Chemistry* **1988**, 263 (36), 19718-19722.
10. Vetter, I. R.; Wittinghofer, A., The guanine nucleotide-binding switch in three dimensions. *Science* **2001**, 294 (5545), 1299-1304.
11. Allin, C.; Ahmadian, M. R.; Wittinghofer, A.; Gerwert, K., Monitoring the GAP catalyzed H-Ras GTPase reaction at atomic resolution in real time. *Proceedings of the National Academy of Sciences* **2001**, 98 (14), 7754-7759.
12. Donovan, S.; Shannon, K. M.; Bollag, G., GTPase activating proteins: critical regulators of intracellular signaling. *Biochimica et biophysica acta* **2002**, 1602 (1), 23-45.
13. Milburn, M. V.; Tong, L.; DeVos, A. M.; Brünger, A.; Yamaizumi, Z.; Nishimura, S.; Kim, S.-H., Molecular switch for signal transduction: structural differences between active and inactive forms of protooncogenic ras proteins. *Science* **1990**, 247 (4945), 939-945.
14. Seabra, M. C., Membrane association and targeting of prenylated Ras-like GTPases. *Cellular signalling* **1998**, 10 (3), 167-172.
15. Cox, A. D.; Der, C. J., Farnesyltransferase inhibitors and cancer treatment: targeting simply Ras? *Biochimica et Biophysica Acta (BBA)-Reviews on Cancer* **1997**, 1333 (1), F51-F71.
16. Okada, T.; Masuda, T.; Shinkai, M.; Kariya, K.-i.; Kataoka, T., Post-translational Modification of H-Ras Is Required for Activation of, but Not for Association with, B-Raf (*). *Journal of biological chemistry* **1996**, 271 (9), 4671-4678.

17. Marshall, C., Specificity of receptor tyrosine kinase signaling: transient versus sustained extracellular signal-regulated kinase activation. *Cell* **1995**, *80* (2), 179-185.
18. Kolch, W., Coordinating ERK/MAPK signalling through scaffolds and inhibitors. *Nature reviews Molecular cell biology* **2005**, *6* (11), 827-837.
19. Downward, J., Targeting RAS signalling pathways in cancer therapy. *Nature reviews cancer* **2003**, *3* (1), 11-22.
20. González-García, A.; Pritchard, C. A.; Paterson, H. F.; Mavria, G.; Stamp, G.; Marshall, C. J., RalGDS is required for tumor formation in a model of skin carcinogenesis. *Cancer cell* **2005**, *7* (3), 219-226.
21. Rangarajan, A.; Hong, S. J.; Gifford, A.; Weinberg, R. A., Species-and cell type-specific requirements for cellular transformation. *Cancer cell* **2004**, *6* (2), 171-183.
22. Muratcioglu, S.; Chavan, T. S.; Freed, B. C.; Jang, H.; Khavrutskii, L.; Freed, R. N.; Dyba, M. A.; Stefanisko, K.; Tarasov, S. G.; Gursoy, A., GTP-dependent K-Ras dimerization. *Structure* **2015**, *23* (7), 1325-1335.
23. Downward, J., Mechanisms and consequences of activation of protein kinase B/Akt. *Current opinion in cell biology* **1998**, *10* (2), 262-267.
24. Khwaja, A., Akt is more than just a Bad kinase. *Nature* **1999**, *401* (6748), 33-34.
25. Rodriguez-Viciana, P.; Warne, P. H.; Dhand, R.; Vanhaesebroeck, B.; Gout, I.; Fry, M. J.; Waterfield, M. D.; Downward, J., Phosphatidylinositol-3-OH kinase direct target of Ras. *Nature* **1994**, *370* (6490), 527-532.
26. Datta, S. R.; Brunet, A.; Greenberg, M. E., Cellular survival: a play in three Akts. *Genes & development* **1999**, *13* (22), 2905-2927.
27. Irani, K.; Xia, Y.; Zweier, J. L.; Sollott, S. J.; Der, C. J.; Fearon, E. R.; Sundaresan, M.; Finkel, T.; Goldschmidt-Clermont, P. J., Mitogenic signaling mediated by oxidants in Ras-transformed fibroblasts. *Science* **1997**, *275* (5306), 1649-1652.
28. Romashkova, J. A.; Makarov, S. S., NF- κ B is a target of AKT in anti-apoptotic PDGF signalling. *Nature* **1999**, *401* (6748), 86-90.
29. Lambert, J. M.; Lambert, Q. T.; Reuther, G. W.; Malliri, A.; Siderovski, D. P.; Sondek, J.; Collard, J. G.; Der, C. J., Tiam1 mediates Ras activation of Rac by a PI (3) K-independent mechanism. *Nature cell biology* **2002**, *4* (8), 621-625.
30. Wolthuis, R. M.; Bos, J. L., Ras caught in another affair: the exchange factors for Ral. *Current opinion in genetics & development* **1999**, *9* (1), 112-117.
31. Tsai, F. D.; Lopes, M. S.; Zhou, M.; Court, H.; Ponce, O.; Fiordalisi, J. J.; Gierut, J. J.; Cox, A. D.; Haigis, K. M.; Philips, M. R., K-Ras4A splice variant is widely expressed in cancer and uses a hybrid membrane-targeting motif. *Proceedings of the National Academy of Sciences* **2015**, *112* (3), 779-784.
32. Oltean, S.; Bates, D. O., Hallmarks of alternative splicing in cancer. *Oncogene* **2014**, *33* (46), 5311-5318.
33. Hobbs, G. A.; Der, C. J.; Rossman, K. L., RAS isoforms and mutations in cancer at a glance. *Journal of Cell Science* **2016**, *129* (7), 1287-1292.
34. Waters, A. M.; Ozkan-Dagliyan, I.; Vaseva, A. V.; Fer, N.; Strathern, L. A.; Hobbs, G. A.; Tessier-Cloutier, B.; Gillette, W. K.; Bagni, R.; Whiteley, G. R., Evaluation of the selectivity and sensitivity of isoform-and mutation-specific RAS antibodies. *Science signaling* **2017**, *10* (498), eaao3332.
35. Hancock, J. F.; Magee, A. I.; Childs, J. E.; Marshall, C. J., All ras proteins are polyisoprenylated but only some are palmitoylated. *Cell* **1989**, *57* (7), 1167-1177.

36. Oliff, A., Farnesyltransferase inhibitors: targeting the molecular basis of cancer. *Biochimica et biophysica acta* **1999**, *1423* (3), C19-30.
37. Simanshu, D. K.; Nissley, D. V.; McCormick, F., RAS proteins and their regulators in human disease. *Cell* **2017**, *170* (1), 17-33.
38. To, M. D.; Wong, C. E.; Karnezis, A. N.; Del Rosario, R.; Di Lauro, R.; Balmain, A., Kras regulatory elements and exon 4A determine mutation specificity in lung cancer. *Nature genetics* **2008**, *40* (10), 1240-1244.
39. Stephen, A. G.; Esposito, D.; Bagni, R. K.; McCormick, F., Dragging ras back in the ring. *Cancer cell* **2014**, *25* (3), 272-281.
40. Cox, A. D.; Der, C. J.; Philips, M. R., Targeting RAS membrane association: back to the future for anti-RAS drug discovery? *Clinical Cancer Research* **2015**, *21* (8), 1819-1827.
41. Prior, I. A.; Hancock, J. F. In *Ras trafficking, localization and compartmentalized signalling*, Seminars in cell & developmental biology, Elsevier: 2012; pp 145-153.
42. Omerovic, J.; Prior, I. A., Compartmentalized signalling: Ras proteins and signalling nanoclusters. *The FEBS journal* **2009**, *276* (7), 1817-1825.
43. Esteban, L. M.; Vicario-Abejón, C.; Fernández-Salguero, P.; Fernández-Medarde, A.; Swaminathan, N.; Yienger, K.; Lopez, E.; Malumbres, M.; McKay, R.; Ward, J. M., Targeted genomic disruption of H-ras and N-ras, individually or in combination, reveals the dispensability of both loci for mouse growth and development. *Molecular and cellular biology* **2001**, *21* (5), 1444-1452.
44. Potenza, N.; Vecchione, C.; Notte, A.; De Rienzo, A.; Rosica, A.; Bauer, L.; Affuso, A.; De Felice, M.; Russo, T.; Poulet, R., Replacement of K-Ras with H-Ras supports normal embryonic development despite inducing cardiovascular pathology in adult mice. *EMBO reports* **2005**, *6* (5), 432-437.
45. Umanoff, H.; Edelmann, W.; Pellicer, A.; Kucherlapati, R., The murine N-ras gene is not essential for growth and development. *Proceedings of the National Academy of Sciences* **1995**, *92* (5), 1709-1713.
46. Quinlan, M. P.; Settleman, J., Isoform-specific ras functions in development and cancer. **2009**.
47. Castellano, E.; Santos, E., Functional specificity of ras isoforms: so similar but so different. *Genes & cancer* **2011**, *2* (3), 216-231.
48. Bos, J. L., Ras oncogenes in human cancer: a review. *Cancer research* **1989**, *49* (17), 4682-4689.
49. Moore, A. R.; Rosenberg, S. C.; McCormick, F.; Malek, S., RAS-targeted therapies: is the undruggable drugged? *Nature Reviews Drug Discovery* **2020**, *19* (8), 533-552.
50. Cerami, E.; Gao, J.; Dogrusoz, U.; Gross, B. E.; Sumer, S. O.; Aksoy, B. A.; Jacobsen, A.; Byrne, C. J.; Heuer, M. L.; Larsson, E., The cBio cancer genomics portal: an open platform for exploring multidimensional cancer genomics data. *Cancer discovery* **2012**, *2* (5), 401-404.
51. Hofmann, M. H.; Gmachl, M.; Ramharter, J.; Savarese, F.; Gerlach, D.; Marszalek, J. R.; Sanderson, M. P.; Kessler, D.; Trapani, F.; Arnhof, H., BI-3406, a Potent and Selective SOS1-KRAS Interaction Inhibitor, Is Effective in KRAS-Driven Cancers through Combined MEK Inhibition Pan-KRAS SOS1 Protein-Protein Interaction Inhibitor BI-3406. *Cancer discovery* **2021**, *11* (1), 142-157.
52. Prior, I. A.; Lewis, P. D.; Mattos, C., A comprehensive survey of Ras mutations in cancer. *Cancer research* **2012**, *72* (10), 2457-2467.

53. Burd, C. E.; Liu, W.; Huynh, M. V.; Waqas, M. A.; Gillahan, J. E.; Clark, K. S.; Fu, K.; Martin, B. L.; Jeck, W. R.; Souroullas, G. P., Mutation-specific RAS oncogenicity explains NRAS codon 61 selection in melanoma. *Cancer discovery* **2014**, *4* (12), 1418-1429.
54. Ihle, N. T.; Byers, L. A.; Kim, E. S.; Saintigny, P.; Lee, J. J.; Blumenschein, G. R.; Tsao, A.; Liu, S.; Larsen, J. E.; Wang, J., Effect of KRAS oncogene substitutions on protein behavior: implications for signaling and clinical outcome. *Journal of the National Cancer Institute* **2012**, *104* (3), 228-239.
55. Vageli, D.; Kiaris, H.; Delakas, D.; Anezinis, P.; Cranidis, A.; Spandidos, D., Transcriptional activation of H-ras, K-ras and N-ras proto-oncogenes in human bladder tumors. *Cancer letters* **1996**, *107* (2), 241-247.
56. Zhou, B.; Der, C. J.; Cox, A. D. In *The role of wild type RAS isoforms in cancer*, Seminars in cell & developmental biology, Elsevier: 2016; pp 60-69.
57. Xu, G.; Lin, B.; Tanaka, K.; Dunn, D.; Wood, D.; Gesteland, R.; White, R.; Weiss, R.; Tamanoi, F., The catalytic domain of the neurofibromatosis type 1 gene product stimulates ras GTPase and complements ira mutants of *S. cerevisiae*. *Cell* **1990**, *63* (4), 835-841.
58. Mendelsohn, J.; Baselga, J., The EGF receptor family as targets for cancer therapy. *Oncogene* **2000**, *19* (56), 6550-6565.
59. von Lintig, F. C.; Dreilinger, A. D.; Varki, N. M.; Wallace, A. M.; Casteel, D. E.; Boss, G. R., Ras activation in human breast cancer. *Breast cancer research and treatment* **2000**, *62* (1), 51-62.
60. Young, A.; Lou, D.; McCormick, F., Oncogenic and Wild-type Ras Play Divergent Roles in the Regulation of Mitogen-Activated Protein Kinase Signaling Regulation of Signaling by Wild-Type and Oncogenic Ras. *Cancer discovery* **2013**, *3* (1), 112-123.
61. Matallanas, D.; Romano, D.; Al-Mulla, F.; O'Neill, E.; Al-Ali, W.; Crespo, P.; Doyle, B.; Nixon, C.; Sansom, O.; Drosten, M., Mutant K-Ras activation of the proapoptotic MST2 pathway is antagonized by wild-type K-Ras. *Molecular cell* **2011**, *44* (6), 893-906.
62. Spiegel, J.; Cromm, P. M.; Zimmermann, G.; Grossmann, T. N.; Waldmann, H., Small-molecule modulation of Ras signaling. *Nature chemical biology* **2014**, *10* (8), 613-622.
63. Khan, I.; Rhett, J. M.; O'Bryan, J. P., Therapeutic targeting of RAS: new hope for drugging the "undruggable". *Biochimica et Biophysica Acta (BBA)-Molecular Cell Research* **2020**, *1867* (2), 118570.
64. Waters, A. M.; Der, C. J., KRAS: the critical driver and therapeutic target for pancreatic cancer. *Cold Spring Harbor perspectives in medicine* **2018**, *8* (9), a031435.
65. Fernández-Medarde, A.; Santos, E., Ras in cancer and developmental diseases. *Genes & cancer* **2011**, *2* (3), 344-358.
66. Ostrem, J. M.; Peters, U.; Sos, M. L.; Wells, J. A.; Shokat, K. M., K-Ras (G12C) inhibitors allosterically control GTP affinity and effector interactions. *Nature* **2013**, *503* (7477), 548-551.
67. Statements, F.-L., Amgen Announces New Clinical Data Evaluating Novel Investigational KRAS (G12C) Inhibitor in Larger Patient Group At WCLC 2019. Barcelona: 2019.
68. Hunter, J. C.; Manandhar, A.; Carrasco, M. A.; Gurbani, D.; Gondi, S.; Westover, K. D., Biochemical and structural analysis of common cancer-associated KRAS mutations. *Molecular cancer research* **2015**, *13* (9), 1325-1335.
69. Janes, M. R.; Zhang, J.; Li, L.-S.; Hansen, R.; Peters, U.; Guo, X.; Chen, Y.; Babbar, A.; Firdaus, S. J.; Darjania, L., Targeting KRAS mutant cancers with a covalent G12C-specific inhibitor. *Cell* **2018**, *172* (3), 578-589. e17.

70. Lanman, B. A.; Allen, J. R.; Allen, J. G.; Amegadzie, A. K.; Ashton, K. S.; Booker, S. K.; Chen, J. J.; Chen, N.; Frohn, M. J.; Goodman, G., Discovery of a covalent inhibitor of KRASG12C (AMG 510) for the treatment of solid tumors. ACS Publications: 2019.
71. Canon, J.; Rex, K.; Saiki, A. Y.; Mohr, C.; Cooke, K.; Bagal, D.; Gaida, K.; Holt, T.; Knutson, C. G.; Koppada, N., The clinical KRAS (G12C) inhibitor AMG 510 drives anti-tumour immunity. *Nature* **2019**, *575* (7781), 217-223.
72. Maciag, A.; Yang, Y.; Turner, D.; Dyba, M.; Kumari, V.; Smith, B.; Fan, L.; Gysin, S.; Wolfe, A.; Abdelkarim, H., Abstract IA21: Preventing KRAS processing. AACR: 2020.
73. Visintin, M.; Tse, E.; Axelson, H.; Rabbitts, T. H.; Cattaneo, A., Selection of antibodies for intracellular function using a two-hybrid in vivo system. *Proceedings of the National Academy of Sciences of the United States of America* **1999**, *96* (21), 11723-11728.
74. Tanaka, T.; Rabbitts, T. H., Protocol for the selection of single-domain antibody fragments by third generation intracellular antibody capture. *Nat Protoc* **2010**, *5* (1), 67-92.
75. Tanaka, T.; Williams, R. L.; Rabbitts, T. H., Tumour prevention by a single antibody domain targeting the interaction of signal transduction proteins with RAS. *The EMBO journal* **2007**, *26* (13), 3250-3259.
76. Tanaka, T.; Rabbitts, T. H., Interfering with protein-protein interactions: potential for cancer therapy. *Cell cycle* **2008**, *7* (11), 1569-1574.
77. Tanaka, T.; Rabbitts, T. H., Intrabodies based on intracellular capture frameworks that bind the RAS protein with high affinity and impair oncogenic transformation. *Embo Journal* **2003**, *22* (5), 1025-1035.
78. Tanaka, T.; Rabbitts, T., Interfering with RAS-effector protein interactions prevent RAS-dependent tumour initiation and causes stop-start control of cancer growth. *Oncogene* **2010**, *29* (45), 6064-6070.
79. Zinzalla, G.; Thurston, D. E., Targeting protein-protein interactions for therapeutic intervention: a challenge for the future. **2009**.
80. Conte, L. L.; Chothia, C.; Janin, J., The atomic structure of protein-protein recognition sites. *Journal of molecular biology* **1999**, *285* (5), 2177-2198.
81. Ward, E. S.; Güssow, D.; Griffiths, A. D.; Jones, P. T.; Winter, G., Binding activities of a repertoire of single immunoglobulin variable domains secreted from Escherichia coli. *Nature* **1989**, *341* (6242), 544-546.
82. Doak, B. C.; Zheng, J.; Dobritzsch, D.; Kihlberg, J., How beyond rule of 5 drugs and clinical candidates bind to their targets. *Journal of medicinal chemistry* **2016**, *59* (6), 2312-2327.
83. Quevedo, C. E.; Cruz-Migoni, A.; Bery, N.; Miller, A.; Tanaka, T.; Petch, D.; Bataille, C. J.; Lee, L. Y.; Fallon, P. S.; Tulmin, H., Small molecule inhibitors of RAS-effector protein interactions derived using an intracellular antibody fragment. *Nature communications* **2018**, *9* (1), 1-12.
84. Cruz-Migoni, A.; Canning, P.; Quevedo, C. E.; Bataille, C. J.; Bery, N.; Miller, A.; Russell, A. J.; Phillips, S. E.; Carr, S. B.; Rabbitts, T. H., Structure-based development of new RAS-effector inhibitors from a combination of active and inactive RAS-binding compounds. *Proceedings of the National Academy of Sciences* **2019**, *116* (7), 2545-2550.
85. Kessler, D.; Gmachl, M.; Mantoulidis, A.; Martin, L. J.; Zoepfel, A.; Mayer, M.; Gollner, A.; Covini, D.; Fischer, S.; Gerstberger, T., Drugging an undruggable pocket on KRAS. *Proceedings of the National Academy of Sciences* **2019**, *116* (32), 15823-15829.
86. Maurer, T.; Garrenton, L. S.; Oh, A.; Pitts, K.; Anderson, D. J.; Skelton, N. J.; Fauber, B. P.; Pan, B.; Malek, S.; Stokoe, D., Small-molecule ligands bind to a distinct pocket in Ras

and inhibit SOS-mediated nucleotide exchange activity. *Proceedings of the National Academy of Sciences* **2012**, *109* (14), 5299-5304.

87. Hillig, R. C.; Sautier, B.; Schroeder, J.; Moosmayer, D.; Hilpmann, A.; Stegmann, C. M.; Werbeck, N. D.; Briem, H.; Boemer, U.; Weiske, J., Discovery of potent SOS1 inhibitors that block RAS activation via disruption of the RAS–SOS1 interaction. *Proceedings of the National Academy of Sciences* **2019**, *116* (7), 2551-2560.

88. Hofmann, M. H.; Gmachl, M.; Ramharter, J.; Savarese, F.; Gerlach, D.; Marszalek, J. R.; Sanderson, M. P.; Kessler, D.; Trapani, F.; Arnhof, H., BI-3406, a potent and selective SOS1–KRAS interaction inhibitor, is effective in KRAS-driven cancers through combined MEK inhibition. *Cancer Discovery* **2021**, *11* (1), 142-157.

89. Ramharter, J.; Kessler, D.; Ettmayer, P.; Hofmann, M. H.; Gerstberger, T.; Gmachl, M.; Wunberg, T.; Kofink, C.; Sanderson, M.; Arnhof, H., One atom makes all the difference: Getting a foot in the door between sos1 and kras. *Journal of Medicinal Chemistry* **2021**, *64* (10), 6569-6580.

90. Shi, Z.-Q.; Yu, D.-H.; Park, M.; Marshall, M.; Feng, G.-S., Molecular mechanism for the Shp-2 tyrosine phosphatase function in promoting growth factor stimulation of Erk activity. *Molecular and cellular biology* **2000**, *20* (5), 1526-1536.

91. Dance, M.; Montagner, A.; Salles, J.-P.; Yart, A.; Raynal, P., The molecular functions of Shp2 in the Ras/Mitogen-activated protein kinase (ERK1/2) pathway. *Cellular signalling* **2008**, *20* (3), 453-459.

92. Chen, Y.-N. P.; LaMarche, M. J.; Chan, H. M.; Fekkes, P.; Garcia-Fortanet, J.; Acker, M. G.; Antonakos, B.; Chen, C. H.-T.; Chen, Z.; Cooke, V. G., Allosteric inhibition of SHP2 phosphatase inhibits cancers driven by receptor tyrosine kinases. *Nature* **2016**, *535* (7610), 148-152.

93. Nichols, R. J.; Haderk, F.; Stahlhut, C.; Schulze, C. J.; Hemmati, G.; Wildes, D.; Tzitzilonis, C.; Mordec, K.; Marquez, A.; Romero, J., RAS nucleotide cycling underlies the SHP2 phosphatase dependence of mutant BRAF-, NF1-and RAS-driven cancers. *Nature cell biology* **2018**, *20* (9), 1064-1073.

94. Ou, S.; Koczywas, M.; Ulahannan, S.; Janne, P.; Pacheco, J.; Burris, H.; McCoach, C.; Wang, J.; Gordon, M.; Haura, E., A12 the SHP2 inhibitor RMC-4630 in patients with KRAS-mutant non-small cell lung cancer: preliminary evaluation of a first-in-man phase 1 clinical trial. *Journal of Thoracic Oncology* **2020**, *15* (2), S15-S16.

95. Berndt, N.; Hamilton, A. D.; Sebti, S. M., Targeting protein prenylation for cancer therapy. *Nature Reviews Cancer* **2011**, *11* (11), 775-791.

96. Bell, I. M., Inhibitors of farnesyltransferase: a rational approach to cancer chemotherapy? *Journal of medicinal chemistry* **2004**, *47* (8), 1869-1878.

97. Sebti, S. M.; Der, C. J., Searching for the elusive targets of farnesyltransferase inhibitors. *Nature Reviews Cancer* **2003**, *3* (12), 945-951.

98. Cox, A. D.; Der, C. J., Farnesyltransferase inhibitors: promises and realities. *Current opinion in pharmacology* **2002**, *2* (4), 388-393.

99. Whyte, D. B.; Kirschmeier, P.; Hockenberry, T. N.; Nunez-Oliva, I.; James, L.; Catino, J. J.; Bishop, W. R.; Pai, J.-K., K-and N-Ras are geranylgeranylated in cells treated with farnesyl protein transferase inhibitors. *Journal of Biological Chemistry* **1997**, *272* (22), 14459-14464.

100. Friday, B. B.; Adjei, A. A., K-ras as a target for cancer therapy. *Biochimica et Biophysica Acta (BBA)-Reviews on Cancer* **2005**, *1756* (2), 127-144.

101. Hatzivassiliou, G.; Song, K.; Yen, I.; Brandhuber, B. J.; Anderson, D. J.; Alvarado, R.; Ludlam, M. J.; Stokoe, D.; Gloor, S. L.; Vigers, G., RAF inhibitors prime wild-type RAF to activate the MAPK pathway and enhance growth. *Nature* **2010**, *464* (7287), 431-435.
102. Kim, T. W.; Lee, J.; Shin, S. J.; Kim, J.-S.; Kim, Y. J.; Han, H. S.; Lee, S. J.; Lim, H.-S.; Hong, Y.-h.; Noh, Y. S., Belvarafenib, a novel pan-RAF inhibitor, in solid tumor patients harboring BRAF, KRAS, or NRAS mutations: Phase I study. American Society of Clinical Oncology: 2019.
103. Desai, J.; Gan, H.; Barrow, C.; Jameson, M.; Atkinson, V.; Haydon, A.; Millward, M.; Begbie, S.; Brown, M.; Markman, B., Phase I, open-label, dose-escalation/dose-expansion study of lifirafenib (BGB-283), an RAF family kinase inhibitor, in patients with solid tumors. *Journal of Clinical Oncology* **2020**, *38* (19), 2140.
104. Dummer, R.; Schadendorf, D.; Ascierto, P. A.; Arance, A.; Dutriaux, C.; Di Giacomo, A. M.; Rutkowski, P.; Del Vecchio, M.; Gutzmer, R.; Mandala, M., Binimetinib versus dacarbazine in patients with advanced NRAS-mutant melanoma (NEMO): a multicentre, open-label, randomised, phase 3 trial. *The Lancet Oncology* **2017**, *18* (4), 435-445.
105. Lito, P.; Saborowski, A.; Yue, J.; Solomon, M.; Joseph, E.; Gadala, S.; Saborowski, M.; Kastenhuber, E.; Fellmann, C.; Ohara, K., Disruption of CRAF-mediated MEK activation is required for effective MEK inhibition in KRAS mutant tumors. *Cancer cell* **2014**, *25* (5), 697-710.
106. Yen, I.; Shanahan, F.; Merchant, M.; Orr, C.; Hunsaker, T.; Durk, M.; La, H.; Zhang, X.; Martin, S. E.; Lin, E., Pharmacological induction of RAS-GTP confers RAF inhibitor sensitivity in KRAS mutant tumors. *Cancer Cell* **2018**, *34* (4), 611-625. e7.
107. Morris, E. J.; Jha, S.; Restaino, C. R.; Dayananth, P.; Zhu, H.; Cooper, A.; Carr, D.; Deng, Y.; Jin, W.; Black, S., Discovery of a novel ERK inhibitor with activity in models of acquired resistance to BRAF and MEK inhibitors. *Cancer discovery* **2013**, *3* (7), 742-750.
108. He, Y.; Li, Y.; Qiu, Z.; Zhou, B.; Shi, S.; Zhang, K.; Luo, Y.; Huang, Q.; Li, W., Identification and validation of PROM1 and CRTC2 mutations in lung cancer patients. *Molecular Cancer* **2014**, *13*, 1-9.
109. Moschos, S. J.; Sullivan, R. J.; Hwu, W.-J.; Ramanathan, R. K.; Adjei, A. A.; Fong, P. C.; Shapira-Frommer, R.; Tawbi, H. A.; Rubino, J.; Rush III, T. S., Development of MK-8353, an orally administered ERK1/2 inhibitor, in patients with advanced solid tumors. *JCI insight* **2018**, *3* (4).
110. Sullivan, R. J.; Infante, J. R.; Janku, F.; Wong, D. J. L.; Sosman, J. A.; Keedy, V.; Patel, M. R.; Shapiro, G. I.; Mier, J. W.; Tolcher, A. W., First-in-Class ERK1/2 Inhibitor Ulixertinib (BVD-523) in Patients with MAPK Mutant Advanced Solid Tumors: Results of a Phase I Dose-Escalation and Expansion StudyPhase I Trial of Ulixertinib, an Oral ERK 1/2 Inhibitor. *Cancer discovery* **2018**, *8* (2), 184-195.
111. Engelman, J. A.; Chen, L.; Tan, X.; Crosby, K.; Guimaraes, A. R.; Upadhyay, R.; Maira, M.; McNamara, K.; Perera, S. A.; Song, Y., Effective use of PI3K and MEK inhibitors to treat mutant Kras G12D and PIK3CA H1047R murine lung cancers. *Nature medicine* **2008**, *14* (12), 1351-1356.
112. Tolcher, A. W.; Khan, K.; Ong, M.; Banerji, U.; Papadimitrakopoulou, V.; Gandara, D. R.; Patnaik, A.; Baird, R. D.; Olmos, D.; Garrett, C. R., Antitumor Activity in RAS-Driven Tumors by Blocking AKT and MEKTargeting KRAS Signaling through MEK and AKT. *Clinical Cancer Research* **2015**, *21* (4), 739-748.
113. Chen, K.; Zhang, Y.; Qian, L.; Wang, P., Emerging strategies to target RAS signaling in human cancer therapy. *Journal of hematology & oncology* **2021**, *14*, 1-23.

114. Johnstone, S.; Albert, J. S., Pharmacological property optimization for allosteric ligands: A medicinal chemistry perspective. *Bioorganic & medicinal chemistry letters* **2017**, *27* (11), 2239-2258.
115. Lawson, A. D.; MacCoss, M.; Heer, J. P., Importance of Rigidity in Designing Small Molecule Drugs To Tackle Protein–Protein Interactions (PPIs) through Stabilization of Desired Conformers: Miniperspective. *Journal of medicinal chemistry* **2017**, *61* (10), 4283-4289.
116. Lea, W. A.; Simeonov, A., Fluorescence polarization assays in small molecule screening. *Expert opinion on drug discovery* **2011**, *6* (1), 17-32.
117. Baker, J. G.; Middleton, R.; Adams, L.; May, L. T.; Briddon, S. J.; Kellam, B.; Hill, S. J., Influence of fluorophore and linker composition on the pharmacology of fluorescent adenosine A1 receptor ligands. *British journal of pharmacology* **2010**, *159* (4), 772-786.
118. Szabó, Á.; Szendi-Szatmári, T.; Ujlaky-Nagy, L.; Rádi, I.; Vereb, G.; Szöllősi, J.; Nagy, P., The effect of fluorophore conjugation on antibody affinity and the photophysical properties of dyes. *Biophysical journal* **2018**, *114* (3), 688-700.
119. Hall, M. D.; Yasgar, A.; Peryea, T.; Braisted, J. C.; Jadhav, A.; Simeonov, A.; Coussens, N. P., Fluorescence polarization assays in high-throughput screening and drug discovery: a review. *Methods and applications in fluorescence* **2016**, *4* (2), 022001.
120. Dempsey, G. T.; Vaughan, J. C.; Chen, K. H.; Bates, M.; Zhuang, X., Evaluation of fluorophores for optimal performance in localization-based super-resolution imaging. *Nature methods* **2011**, *8* (12), 1027-1036.
121. Simeonov, A.; Jadhav, A.; Thomas, C. J.; Wang, Y.; Huang, R.; Southall, N. T.; Shinn, P.; Smith, J.; Austin, C. P.; Auld, D. S., Fluorescence spectroscopic profiling of compound libraries. *Journal of medicinal chemistry* **2008**, *51* (8), 2363-2371.
122. Turek-Etienne, T. C.; Small, E. C.; Soh, S. C.; Xin, T. A.; Gaitonde, P. V.; Barrabee, E. B.; Hart, R. F.; Bryant, R. W., Evaluation of fluorescent compound interference in 4 fluorescence polarization assays: 2 kinases, 1 protease, and 1 phosphatase. *Journal of biomolecular screening* **2003**, *8* (2), 176-184.
123. Miyaura, N.; Suzuki, A., Palladium-catalyzed cross-coupling reactions of organoboron compounds. *Chemical reviews* **1995**, *95* (7), 2457-2483.
124. Guram, A. S.; Rennels, R. A.; Buchwald, S. L., A simple catalytic method for the conversion of aryl bromides to arylamines. *Angewandte Chemie International Edition in English* **1995**, *34* (12), 1348-1350.
125. Tanaka, T.; Thomas, J.; Van Montfort, R.; Miller, A.; Rabbitts, T., Pan RAS-binding compounds selected from a chemical library by inhibiting interaction between RAS and a reduced affinity intracellular antibody. *Scientific reports* **2021**, *11* (1), 1-10.
126. Zhu, M.-r.; Du, D.-h.; Hu, J.-c.; Li, L.-c.; Liu, J.-q.; Ding, H.; Kong, X.-q.; Jiang, H.-l.; Chen, K.-x.; Luo, C., Development of a high-throughput fluorescence polarization assay for the discovery of EZH2-EED interaction inhibitors. *Acta Pharmacologica Sinica* **2018**, *39* (2), 302-310.
127. Kong, X.; Chen, L.; Jiao, L.; Jiang, X.; Lian, F.; Lu, J.; Zhu, K.; Du, D.; Liu, J.; Ding, H., Astemizole arrests the proliferation of cancer cells by disrupting the EZH2-EED interaction of polycomb repressive complex 2. *Journal of medicinal chemistry* **2014**, *57* (22), 9512-9521.
128. Zhou, W.; Li, Y.; Song, J.; Li, C., Fluorescence polarization assay for the identification and evaluation of inhibitors at YAP–TEAD protein–protein interface 3. *Analytical biochemistry* **2019**, *586*, 113413.

129. Graves, T. L.; Zhang, Y.; Scott, J. E., A universal competitive fluorescence polarization activity assay for S-adenosylmethionine utilizing methyltransferases. *Analytical biochemistry* **2008**, 373 (2), 296-306.